A Model that Predicts the Material Recognition Performance of Thermal Tactile Sensing

The International Journal of Robotics Research
XX(X):1–19

DOI: 10.1177/ToBeAssigned
www.sagepub.com/
SAGE

Tapomayukh Bhattacharjee[1], Haoping Bai[1], Haofeng Chen[1], and Charles C. Kemp[1]

Abstract
Tactile sensing can enable a robot to infer properties of its surroundings, such as the material of an object. Heat transfer based sensing can be used for material recognition due to differences in the thermal properties of materials. While data-driven methods have shown promise for this recognition problem, many factors can influence performance, including sensor noise, the initial temperatures of the sensor and the object, the thermal effusivities of the materials, and the duration of contact. We present a physics-based mathematical model that predicts material recognition performance given these factors. Our model uses semi-infinite solids and a statistical method to calculate an F_1 score for the binary material recognition. We evaluated our method using simulated contact with 69 materials and data collected by a real robot with 12 materials. Our model predicted the material recognition performance of support vector machine (SVM) with 96% accuracy for the simulated data, with 92% accuracy for real-world data with constant initial sensor temperatures, and with 91% accuracy for real-world data with varied initial sensor temperatures. Using our model, we also provide insight into the roles of various factors on recognition performance, such as the temperature difference between the sensor and the object. Overall, our results suggest that our model could be used to help design better thermal sensors for robots and enable robots to use them more effectively.

Keywords
Haptics, Tactile Sensing, Heat Transfer, Material Recognition, Physics-based Modeling.

1 INTRODUCTION

Material recognition using thermal sensing is relatively unexplored in robotics when compared with other haptic sensing modalities such as force sensing. Under some conditions, robots can use this sensing modality to recognize contact with materials that have distinct thermal properties (Bhattacharjee et al. 2015). Recognizing the material when a robot touches an object can help in devising intelligent manipulation strategies. For example, a robot might come in contact with a bed or a mattress while assisting a person with disabilities who is in bed. Recognizing that the object in contact is 'wood' might help a robot infer that it is in contact with the bed frame instead of the human body or the mattress and thus, the robot might alter its actions. For example, we have shown the relevance of recognizing 'tactile foreground' vs. 'tactile background' for task-specific manipulation tasks (Bhattacharjee et al. 2016), where 'tactile foreground' is the target object and 'tactile background' is any other object in its vicinity that the robot may come in contact with during the manipulation task.

However, the performance of material recognition with thermal tactile sensing varies considerably. We present a mathematical model that predicts the performance of material recognition based on a number of factors. Specifically, our model predicts the F_1 score for binary material recognition given properties of the object, the sensor, the environment, and the contact made between the object and the sensor. We also use this model to predict material recognition performance across a set of objects. In contrast to a strictly empirical approach to estimating material recognition performance, our mathematical model provides performance predictions without the resource-intensive process of collecting data and does so for a large set of physically-meaningful parameters. This can be useful for a number of pursuits, including sensor design and algorithm design. It also can help give people intuition for active thermal sensing. This could be especially valuable since active thermal sensing has been a less prevalent and less widely understood sensing modality in robotics compared to modalities such as audition, vision, and force sensing. For example, in contrast to active thermal sensing, people often have intuitions for the implications of common phenomena in machine vision, such as low light environments, a camera's field of view, an unfocused lens, and objects that look similar to one another.

Our model considers heat transfer based thermal sensing, which involves a tactile sensor with a heating element and a temperature sensor touching an object. We refer to this as 'active' thermal sensing in contrast to 'passive' thermal sensing, which we use to refer to a temperature sensor

[1]Healthcare Robotics Lab, Institute for Robotics and Intelligent Machines, Georgia Institute of Technology

Corresponding author:
Tapomayukh Bhattacharjee, Healthcare Robotics Laboratory, Institute for Robotics and Intelligent Machines, Georgia Institute of Technology, 313 Ferst Drive, Atlanta, GA-30332, USA.
Email: tapomayukh@gatech.edu

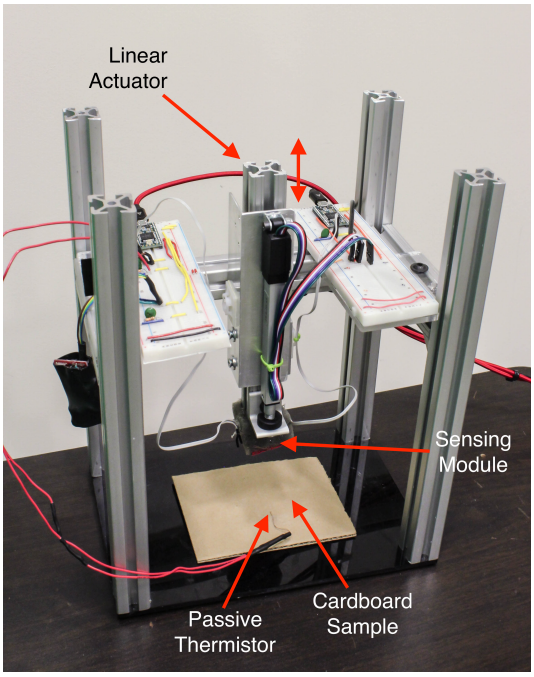

Figure 1. *A 1-DoF Robot with an active thermal sensing module reaching to touch a cardboard material sample*

alone making contact with an object. During active thermal sensing, when the tactile sensor, which is heated above room temperature, comes in contact with an object at room temperature, heat transfers away from the sensor into the object. This heat transfer is dependent on the sensor and object thermal properties, the initial temperature conditions of the sensor and the object, as well as the noise due to various sensor and environmental conditions. A robot can sometimes use the difference in this heat transfer for different materials to distinguish them.

We developed a physics-based model using a semi-infinite solid assumption for modeling heat transfer from the heated sensor to the object. We added Gaussian i.i.d noise to model the effect of noise. This model can account for the variability in the initial conditions of the sensor and the object, the sensor and object thermal properties, as well as noise. Using this model, we can generate simulated time-series heat transfer data given sensor and object parameters as well as their initial temperature conditions. We modeled this time-series as Gaussian process and developed a statistical method to calculate the F_1 score of the binary material recognition performance. Using this model and the statistical method, we analyzed the effect of material thermal effusivities, initial temperatures, and noise on the material recognition performance. Given material properties, environmental conditions and a desired level of material recognition performance, this model could potentially be used to help provide design guidelines for thermal sensors. We also estimated the binary material recognition performance for all materials in the CES Edupack Level-1 Database (Ashby 2008) resulting in a total of 2346 binary material recognition tasks and compared the results with that of Support Vector Machine (SVM). We also collected data from 12 real-world representative materials using a 1-DOF robot with a linear actuator and a tactile sensor attached at its end (see Figure 1). We estimated their material recognition performance (66 binary comparisons) using the identified parameters from the real-world data, the physics-based model, and the statistical method. Our objective was to see if our model could predict the results obtained using SVM.

2 RELATED WORK

In predicting perception performance of sensor systems, sensor specifications alone often fail to provide an insightful understanding of the entire system. Thus, modeling the effect of various low-level factors, such as noise, on the overall system performance for specific tasks is important for a holistic understanding of the system. Such understanding can provide useful guidelines for designing a sensor to achieve a desired performance in a specific task. Researchers have established such end-to-end understanding over a wide range of sensor systems, including system robustness measure (Petrovi and Xydeas 2000) and performance visualization (Gow et al. 2007) of imaging systems with CMOS sensor, target acquisition performance with infrared imager (Krapels et al. 2007), and TOD-sensor performance curve prediction for multiple sensor systems (Hogervorst et al. 2001).

In this work, we develop an end-to-end analytical performance model that uses a physics-based heat transfer model and a statistical method to understand the effect of sensor properties and environmental conditions on material recognition tasks. We demonstrate the potential of using our statistical model to guide the choice of sensor design parameters for material recognition tasks using thermal sensing modality.

In this section, we first focus on relevant heat transfer models as the essential grounds for our work. We then present a review of relevant thermal sensing sensors as well as their use for material recognition and other applications.

2.1 Heat Transfer Modeling

Researchers have modeled heat transfer between a human finger and an object as heat transfer between two semi-infinite solids (See Section 4.1) and used this model to simulate heat transfer for thermal displays (Ho and Jones 2004; Yamamoto et al. 2004). Researchers have also used this model for the measurement of thermal properties of objects when a thermal sensor touches an object (Fudym et al. 2005; Jannot and Meukam 2004). For real-world heat transfer between two objects, however, the semi-infinite solid model is valid for a short duration after contact (Lienhard 2011). In our work, because we attempt to recognize materials with a short contact duration of 1s-4s, we used the semi-infinite solid model in our experiments.

Ho and Jones (2004) developed a thermal display to simulate the temperature of different surfaces after being in contact with fingers. They employed a semi-infinite solid model for the display and compared it to real materials. They used 5 materials for the thermal display with ten adults as subjects and claimed that there is no significant difference between real and simulated materials when recognized by human subjects. Benali-Khoudjal et al. (2003) developed a heat transfer model between human fingers and different surfaces based on an electrical analogy. They modeled the

finger and the material as blocs with electrical components and ran simulations to compare with real experiments.

Jones and Ho (2008); Ho and Jones (2006, 2008) suggested that the semi-infinite solid model does not take thermal contact resistance into account. Thermal contact resistance changes with contact force and affects the temperature response. They incorporated thermal contact resistance into the semi-infinite solid model and claimed that the model makes the temperature responses more realistic. Yamamoto et al. (2004) developed a thermal tactile display with the control of temperature based on the semi-infinite solid model. They claimed that the thermal contact resistance is negligible with enough contact force of 600 gf. With enough contact force in our experiments, we assume that thermal contact resistance is negligible.

In our study, we model the heat transfer between the sensor and the material sample as contact between two semi-infinite solids. Although relevant studies used the semi-infinite solid assumption to model heat transfer, they did not use the heat transfer model to develop an end-to-end statistical model of material recognition performance. Our developed model can guide the choice of suitable sensor parameters needed to obtain a desired material recognition performance using the thermal sensing modality. In addition, we tested our model with a wide and diverse set of materials through both simulations as well as experiments for material recognition tasks.

In the next section, we will review different thermal sensors used in the literature and their application to relevant material recognition tasks, if any.

2.2 Thermal Sensing

2.2.1 Passive Thermal Sensing A passive thermal sensor measures the temperature of a target object without introducing additional heat source. Related work on passive thermal sensors is more hardware-centric with limited applications in material detection. In this section, we will discuss both contact-based and non-contact-based passive thermal sensors.

Contact-Based Sensors

Researchers used different types of contact-based thermal sensors to develop passive sensing devices. Contact-based thermal sensors fall into three categories: Resistance Temperature Detectors (RTDs), Thermistors and Thermocouples. RTDs and Thermistors measure temperature using the phenomenon that the resistance of some materials changes as temperature changes. Thermocouples function by the Seebeck Effect (Herwaarden and Sarro 1986), which states that the difference between temperatures of two electric junctions in a thermoelectric device creates a voltage. Of the three types of thermal sensors, thermocouples have the widest operating range of -200°C to 2000°C, with relatively low accuracy. RTDs have a high accuracy of 0.03°C with relatively long response time. Compared with RTDs, thermistors have a lower accuracy of 0.1°C but give faster thermal responses (Tong 2001).

Many researchers (Caselli et al. 1994; Yang et al. 2010, 2008b; Someya et al. 2005; Castelli 1995; Hedengren et al. 2001; Shih et al. 2010; Ma et al. 2010) developed arrays of combined thermal and tactile sensors using RTDs and thermistors. Someya et al. (2005) developed a flexible artificial electronic skin with a network of pressure and thermal sensors using organic diodes. They pointed out that the network can be applied on robot fingers, but they did not mention its application on material recognition. Ma et al. (2010) fabricated a flexible thermal sensor array using Nickel-based RTDs to detect dynamic wave flow in hydrodynamic experiments. Bayindir et al. (2006) developed a fiber device for large area thermal sensing, using long fiber thermistors that can sense heat along its entire length and generate electrical signals in response.

Non-Contact-Based Sensors

An alternative type of passive thermal sensor is non-contact-based, which detects the radiated energy out of the target object by applying the Planck's Law of Radiation (Planck 2013). By avoiding contact, such sensors have the advantage of real-time nondestructive measurement. A common type of non-contact-based thermal sensor is the infrared camera. Many researchers study complex heat transfer problems by taking advantage of infrared cameras (Kabov and Marchuk 1996; Matian et al. 2010; Boukhanouf et al. 2006). Sarro et al. (1988) developed an infrared thermal sensing linear array based on integrated silicon thermopiles, and Schaufelbuhl et al. (2001) fabricated a thermal imager consisting of a 10×10 array of infrared sensors. Both claim that their designs have the advantage of low cost, low crosstalk, and high yield, and can be applied to monochromatic radiation sensing.

In summary, studies on passive thermal sensing focus on the fabrication process of sensing hardware, with limited evaluation for inferring thermal properties of materials or objects.

2.2.2 Active Thermal Sensing Active thermal sensors have a heating element to heat up the sensor above room temperature and a thermistor to measure the response over time. Thus, on contact with an object at room temperature, there is heat transfer away from the sensor into the object. Unlike the passive thermal sensing modality, researchers have used active thermal sensing modality for material recognition purposes as well.

Contact-Based Sensors

a. RTDs and Thermistors Many researchers used heated thermistors and RTDs to develop integrated thermal and tactile sensing systems (Russell 1985; Siegel et al. 1986; Engel et al. 2005, 2006; Takamuku et al. 2008; Liu et al. 2008; Mansky and Bennett 2002; Yuji and Shida 2000; Mansky and Bennett 2003; Dario et al. 1984; Dario and De Rossi 1985; Taddeucci et al. 1997; Mittendorfer and Cheng 2011; Kim et al. 2014). Russell (1985) developed an array of thermistors, with which he compared the percent decrease of different materials from a uniform initial temperature. The array recognized six different materials using the temperature after 3 seconds of contact in a single trial. Siegel et al. (1986) developed an integrated tactile and thermal sensor, and compared the response of the thermistor on wood, nylon, and steel over a 50 second period, with the initial temperature maintained using the heat generated by current flow on the conductive paint. They performed material recognition by matching the sensor's response with an existing library of response curves.

Engel et al. (2005, 2006) developed flexible multimodal tactile sensing systems with gold heaters and nickel RTDs. With consistent initial conditions and based on the combined pressure and temperature sensing, their system successfully identified five materials with 90% accuracy over 50 trials and unreported contact duration. Takamuku et al. (2008) developed an anthropomorphic finger with three strain gauges, four thermistors and a heating element in a layered format. They used the outputs of thermal and tactile sensors to classify five different materials.

In the study of multimodal material recognition, researchers expressed the need for thermal sensing (Wettels et al. 2008), which led to the development of the multimodal SynTouch BioTAC sensor (Syntouch 2015). Some researchers also used the thermal modality in the multimodal SynTouch BioTAC sensor (Syntouch 2015) for material recognition. Xu et al. (2013) used the BioTAC sensor to measure the temperature derivative and other multimodal sensor data during 15 s of contact. They used Bayesian exploration and reinforcement learning techniques to identify ten objects with 99% accuracy using the data. Chu et al. (2015); McMahon et al. (2012) used the BioTAC sensor on a PR2 robot to collect multimodal (including thermal) haptic data for recognizing haptic adjectives. They used discrete HMMs to construct a feature vector of likelihoods and used binary SVM classifiers to classify those vectors and automatically assign 24 adjectives to 60 objects. Their research focused on classifying data using both static and dynamic features from four deliberate exploratory procedures with sophisticated BioTac (Lin et al. 2009) robotic fingers from *Syntouch*. Kerr et al. (2013) used the BioTAC sensor to record the thermal response data of six material groups for 20 s. They used the derivative of the temperature (TAC) as well as the dynamic thermal conductivity (TDC) data and got 73% accuracy with artificial neural networks.

b. Thermocouples Of the three types of contact-based thermal sensors, thermocouples generally have relatively faster responses, wider range but lower accuracy (Tong 2001). Monkman and Taylor (1993) developed a method of using the response drive current of a thermocouple in performing material recognition, which they reported to be faster than that of Russell (1985) and Siegel et al. (1986). They evaluated the sensor by recognizing four materials with distinct thermal properties under consistent initial conditions. Their results from sensor readings over time of a single trial suggest that the recognition of the four materials could potentially be performed more quickly (between 0 and 3 s), but they did not report specific results.

Caldwell and Gray (1993) developed a method of using the response output voltage of a thermocouple in material recognition while maintaining the temperature of the sensor at 40 ± 0.5 °C. They collected data for seven materials with 20 trials each and showed a graph of the probability densities of the seven materials for steady-state thermocouple output voltage. However, they did not apply the sensor data to any classification algorithm to get the performance of material recognition. Caldwell and Gosney (1993) proposed a multifunctional tactile sensor, in which they used thermocouples to acquire temperature gradient information through induced output voltage. They reported high accuracy for classifying five materials using the thermal sensing modality, but they did not report the specific classification method used.

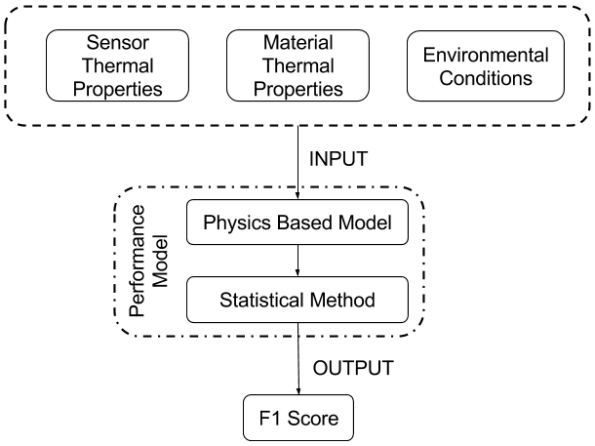

Figure 2. *Schematic of our Performance model*

Jackson W. proposed a paper sensing system that identified physical properties of papers. The system included a heater and two thermocouples to detect the thermal diffusivity of different papers (Jackson et al. 1999). Shao et al. (2010) developed a measurement system with thermocouples in the thermal module. The system served to quantify human sensory perceptions by studying the correlation of collected sensor data and human subject self-report data. A similar attempt to quantify human haptic perception (Chen et al. 2009) also used thermocouples to simulate human contact of materials and register the thermal process.

Non-Contact-Based Sensors

Though not often used in material recognition, non-contact-based thermal sensors also have application in active thermal sensing. An example is the method of Infrared Non-destructive Testing (IRNDT) (Kaplan 2007) to find defects in laminar materials. The method injects controlled thermal energy into the test sample and uses infrared cameras to observe the response. Mulaveesala et al. (2013) applied different non-stationary thermal excitation schemes to perform IRNDT on fiber-reinforced plastic materials. VanDamme and McGarvey (1972) performed IRNDT on various laminate materials and electric circuits to detect flaws using infrared lamp and low-power CO_2 laser heat source.

In summary, related studies using contact-based active thermal sensing performed material recognition on small sets of materials with various data-driven machine learning algorithms. However, they did not make use of heat transfer models to develop an end-to-end statistical model that can predict recognition performance of materials with arbitrary thermal properties.

3 A MODEL FOR PERFORMANCE PREDICTION

In our attempt to better understand material recognition using thermal sensing, we derived a performance model that, given a set of sensor and environmental conditions, evaluates the expected performance of a material recognition task. Our model calculates the probability of successfully distinguishing two materials, given the thermal properties

of a sensor and a material sample as well as environmental conditions.

Figure 2 shows our approach for the performance model. It consists of a physics-based model (Bhattacharjee et al. 2015) that takes sensor and material thermal properties as well as environmental conditions as inputs and outputs a time-series heat transfer data. This heat transfer data is then fed into a statistical method which helps quantify the difference between the heat transfer data from two materials. We express this difference in terms of F_1 scores.

4 PHYSICS-BASED MODEL

Here we present a physics-based model of the heat transfer process between a heated sensor and a material sample.

4.1 Semi-infinite Solid Model

A semi-infinite solid is an idealized body in which a temperature change in any part of the body is due to thermal conditions on a single surface (Yunus and Afshin 2010). Yunus and Afshin (2010) has modeled a finger touching a material sample as a contact between two semi-infinite bodies. In an analogous manner, we modeled the heat transfer process between a heated thermal sensor and a block of material as heat conduction between two semi-infinite solids (Yunus and Afshin 2010; Mathis 2000). Figure 3 shows the diagram that represents this model.

In the model, we first assume that the initial temperature of the object, $T_{obj(t=0)}$, is equal to the ambient temperature, T_{amb}. The initial temperature of the sensor, $T_{sens}(t=0)$, is higher than T_{amb}.

Once the sensor comes into contact with the object, heat begins to transfer from the sensor to the object, resulting in temperature change over time. In the sensor, let x be the distance of the thermistor from the contact surface (Fig. 3). The contact surface at $x=0$ has a temperature T_{surf} that remains constant and is given by

$$T_{surf} = \frac{(T_{sens}(t=0)e_{sens} + T_{obj}(t=0)e_{obj})}{(e_{sens}+e_{obj})}$$
$$where \quad e_{sens} = \frac{k_{sens}}{\sqrt{\alpha_{sens}}} \quad and \quad e_{obj} = \frac{k_{obj}}{\sqrt{\alpha_{obj}}} \tag{1}$$

where α_{obj} and k_{obj} are the coefficients of thermal diffusivity and thermal conductivity of the object respectively, and α_{sens} and k_{sens} are the coefficients of thermal diffusivity and thermal conductivity of the sensor respectively. Given $T_{sens}(t=0)$ and T_{surf}, we can find the temperature in the sensor at any time, $t \geq 0$, using the following partial differential equation from Yunus and Afshin (2010):

$$\frac{\partial^2 T_{sens}}{\partial x^2} = \frac{1}{\alpha_{sens}} \frac{\partial T_{sens}}{\partial t} \tag{2}$$

where $T_{sens}(x,t)$ is the temperature at time t of the sensor at distance x from the contact surface. The thermistor, which is inside the sensor, measures the temperature at $x = 8 * 10^{-5}$ (obtained from manufacturer) as shown in Fig. 3. Using the boundary conditions, $T_{sens}(x=0,t) = T_{surf}$ and $T_{sens}(x, t=0) = T_{sens}(t=0)$, we can solve for $T_{sens}(x,t)$.

$$T_{sens}(x,t) = T_{sens}(t=0) + (T_{surf} - T_{sens}(t=0)) \times erfc\left(\frac{x}{2\sqrt{\alpha_{sens} t}}\right) \tag{3}$$

where $erfc$ is the complimentary error function given by

$$erfc(z) = \frac{2}{\sqrt{\pi}} \int_z^\infty e^{-r^2} dr \tag{4}$$

With the physics based model we can predict the sensor readings, $T_{sens}(x = 8 \times 10^{-5}, t)$, that would result from the heat transfer when the tactile sensor comes in contact with a material sample with thermal effusivity e_{obj}.

4.2 Noise Model

Note that during each temperature measurement, the measurement of the sensor also includes noise and other sources of uncertainty. In order to account for the noise and uncertainty in sensor reading, we introduce an additive Gaussian noise, Z_i, with zero mean and variance σ^2 to each temperature measurement. The underlying assumption is that, the deviation of each sensor reading from the actual sensor temperature, caused by the uncertainty due to various conditions, can be modeled as an independent normal random variable.

With noise taken into consideration, the final sensor model is given by

$$T_{sens}(x,t) = T_{sens}(t=0) + (T_{surf} - T_{sens}(t=0)) * erfc\left(\frac{x}{2\sqrt{\alpha_{sens} t}}\right) + Z \sim \mathcal{N}\left(0, \sigma^2\right) \tag{5}$$

This modified model can help us analyze the effect of noise on the performance of material recognition.

5 STATISTICAL METHOD

In this section, we derive a performance model to evaluate material recognition performance when a sensor touches two different materials under specific environmental conditions and noise.

5.1 Gaussian Process

In order to account for the effect of noise, we first explain the concept of Gaussian Process (GP). In a Gaussian process, every point in some continuous input space is associated with a normally distributed random variable. The distribution of a Gaussian process is the joint distribution of all those (infinitely many) random variables, and as such, it is a distribution over functions in a continuous domain (Frigola-Alcade 2015). In our case, the continuous domain is time, and every time instant is associated with a normal random variable. If we choose to sample at any particular instant, we are essentially sampling from the normal random variable

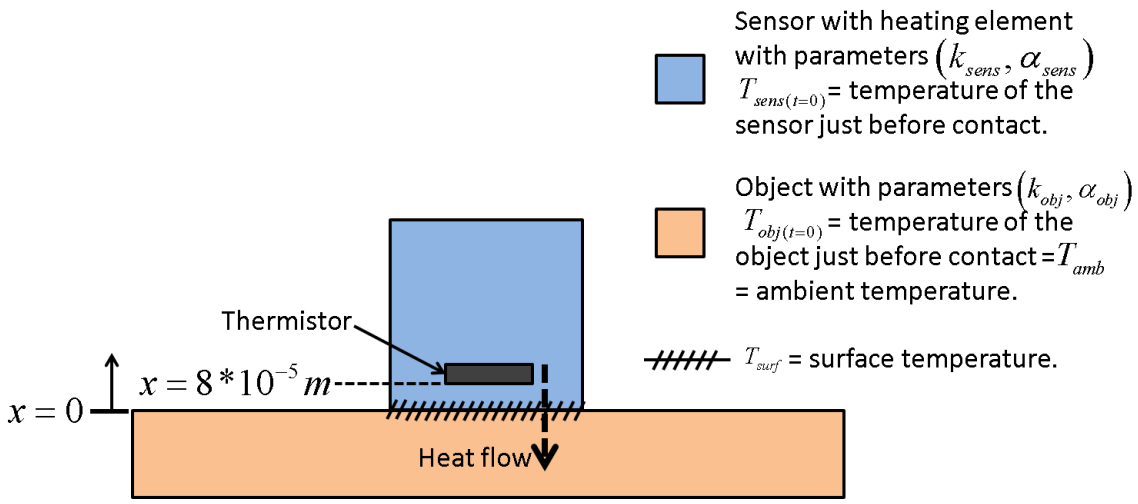

Figure 3. *Diagram representing our model of the sensor in contact with a material sample. We model both the sensor and the material sample as semi-infinite solids.*

associated with that instant. Although in practice, we only sample a finite collection (time series) of observations, the distribution of the collection (time series) is still the joint distribution of all the observations within the collection, which results in a multivariate normal distribution.

In our model, let T_{sens} be the random function (given by Eq. 5, with x fixed) from which every observation $T_{sens}(t_i)$ can be sampled. We have

$$T_{sens}(t_i) = f(t_i) + \epsilon_i \sim i.i.d.\mathcal{N}\left(0, \sigma^2\right) \tag{6}$$

where $f(t)$ is the mean function (given by Eq. 3) and ϵ_i is a random normal variable.

Thus, we can express T_{sens} as Gaussian process $GP(f, K)$, which implies that the random function T_{sens} is distributed as a GP with mean function f and covariance function K (Rasmussen 2004). The covariance for any two given samples is given by K as

$$\begin{aligned} & K(T_{sens}(t_i), T_{sens}(t_j)) \\ &= COV(T_{sens}(t_i), T_{sens}(t_j)) \\ &= \mathbb{E}\big[T_{sens}(t_i) - \mathbb{E}[T_{sens}(t_i)]\big] * \\ &\quad \mathbb{E}\big[T_{sens}(t_j) - \mathbb{E}[T_{sens}(t_j)]\big] \\ &= \mathbb{E}\big[f(t_i) + \epsilon_i - f(t_i)\big] * \\ &\quad \mathbb{E}\big[f(t_j) + \epsilon_j - f(t_j)\big] \\ &= \mathbb{E}\big[\epsilon_i\big]\mathbb{E}\big[\epsilon_j\big] \end{aligned} \tag{7}$$

Since $\epsilon_i, \epsilon_j \sim i.i.d.\mathcal{N}\left(0, \sigma^2\right)$,

$$K(T_{sens}(t_i), T_{sens}(t_j)) = \mathbb{E}\big[\epsilon_i \epsilon_j\big] \tag{8}$$

5.2 Multivariate Normal Distribution

The multivariate normal distribution $\mathcal{N}(\boldsymbol{\mu}, \boldsymbol{\Sigma})$ is a generalization of the one-dimensional (univariate) normal distribution to higher dimensions, given as

$$P(\boldsymbol{x}|\boldsymbol{\mu}, \boldsymbol{\Sigma}) = \frac{1}{\sqrt{(2\pi)^n |\boldsymbol{\Sigma}|}} \exp\left(-\frac{1}{2}(\boldsymbol{x} - \boldsymbol{\mu})^T \boldsymbol{\Sigma}^{-1} (\boldsymbol{x} - \boldsymbol{\mu})\right) \tag{9}$$

where $\boldsymbol{x}$ is an n dimensional random vector, $\boldsymbol{\mu}$ is the n dimensional mean vector given by $\mathbb{E}[\boldsymbol{x}] = \{f(t_i)|i \in (1, n)\}$ (f being the mean function), and $\boldsymbol{\Sigma}$ is the $n \times n$ covariance matrix.

Every set of finite samples $\boldsymbol{x} = \{T_{sens}(t_i)|i \in (1, n)\}$ drawn from $T_{sens} = GP(f, K)$ can be viewed as a random vector corresponding to a multivariate normal distribution. Thus, we can calculate the probability of observing a specific random vector $\boldsymbol{x}$ given prior knowledge of the mean function and the covariance matrix.

Also, the covariance function K is a spherical covariance matrix for the random vector $\boldsymbol{x}$:

$$\boldsymbol{\Sigma}_{ij} = \mathbb{E}\big[\epsilon_i \epsilon_j\big] = \begin{cases} \sigma^2 & i = j \\ 0 & i \neq j \end{cases} \tag{10}$$

As a result, $\boldsymbol{\Sigma}$ is a diagonal matrix in which the main diagonal entries are all σ^2. Thus, we have the determinant of $\boldsymbol{\Sigma}$ equal to the product of all main diagonal entries

$$|\boldsymbol{\Sigma}| = (\sigma^2)^n \tag{11}$$

Rewriting the probability distribution function, we have

$$P(\boldsymbol{x}|\boldsymbol{\mu}, \boldsymbol{\Sigma}) = \frac{1}{\sqrt{(2\pi\sigma^2)^n}} \exp\left(-\frac{1}{2}(\boldsymbol{x} - \boldsymbol{\mu})^T (\boldsymbol{x} - \boldsymbol{\mu})/\sigma^2\right) \tag{12}$$

Eq.12 represents the probability distribution of observed measured time series $\boldsymbol{x}$, given the mean vector $\boldsymbol{\mu}$ and covariance matrix $\boldsymbol{\Sigma}$ associated with the underlying Gaussian process $T_{sens} = GP(f, K)$.

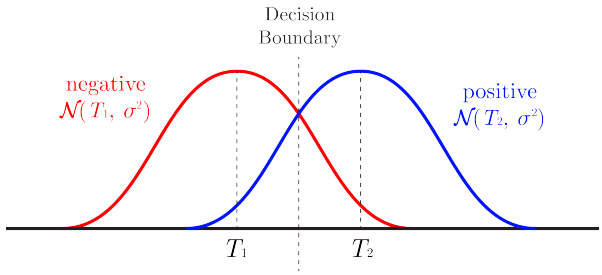

Figure 4. *Gaussian Decision Boundary illustrated in 1 Dimension*

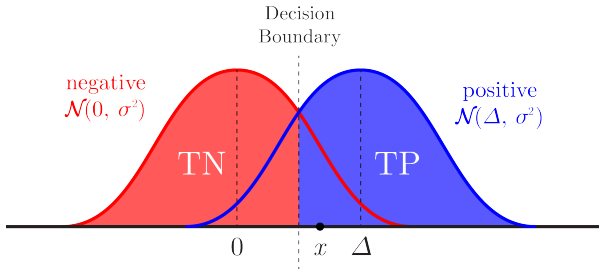

Figure 5. *True Negative Rate and True Positive Rate*

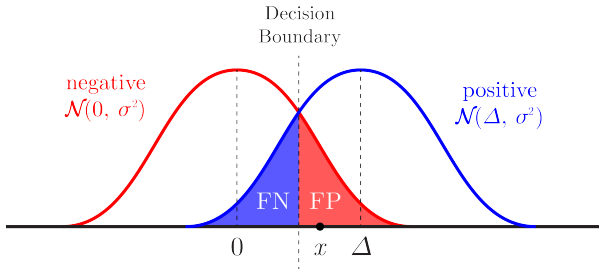

Figure 6. *False Negative Rate and False Positive Rate*

5.3 F_1 score and F_1 score Matrix

We determine whether a given material pair is distinguishable by modeling the performance of a binary classifier given a random time series sample from each of the two materials. We sample the time-series data from the underlying multivariate normal distribution associated with each of the two materials. In other words, if the labeling accuracy of the binary classifier is higher than a certain threshold, we decide that the material pair is distinguishable. For consistency, we use F_1 score as the accuracy measurement and 0.9 as the threshold.

We model the decision process of binary classifiers with a Gaussian decision boundary. Consider two underlying distributions of random vector variables (time series) $\boldsymbol{\mathcal{N}}(\boldsymbol{T}_1, \boldsymbol{\Sigma})$ and $\boldsymbol{\mathcal{N}}(\boldsymbol{T}_2, \boldsymbol{\Sigma})$ each associated with a material sample. At any instant, we obtain a sensor measured time series vector $\boldsymbol{x}'$, and we want to label it with its corresponding material label. Since we actually do not know which material the sensor is currently in contact with, we label $\boldsymbol{x}'$ with the more probable distribution by comparing $P(\boldsymbol{x}'|\boldsymbol{T}_1, \boldsymbol{\Sigma})$ and $P(\boldsymbol{x}'|\boldsymbol{T}_2, \boldsymbol{\Sigma})$, and assign the more probable label. This leads to the formation of a decision boundary as illustrated in Fig. 4, which is a hyperplane in the n dimensional space associated with the two distributions. To simplify the calculation, we translate both distributions by $-\boldsymbol{T}_1$, and define $\boldsymbol{x} = \boldsymbol{x}' - \boldsymbol{T}_1$, $\boldsymbol{\Delta} = \boldsymbol{T}_2 - \boldsymbol{T}_1$.

We can then express the translated distributions as $\boldsymbol{\mathcal{N}}(\boldsymbol{0}, \boldsymbol{\Sigma}) = \boldsymbol{\mathcal{N}}(\boldsymbol{T}_1 - \boldsymbol{T}_1, \boldsymbol{\Sigma})$ and $\boldsymbol{\mathcal{N}}(\boldsymbol{\Delta}, \boldsymbol{\Sigma}) = \boldsymbol{\mathcal{N}}(\boldsymbol{T}_2 - \boldsymbol{T}_1, \boldsymbol{\Sigma})$. As a result, $P(\boldsymbol{x}'|\boldsymbol{T}_1, \boldsymbol{\Sigma}) = P(\boldsymbol{x}|\boldsymbol{0}, \boldsymbol{\Sigma})$, and $P(\boldsymbol{x}'|\boldsymbol{T}_2, \boldsymbol{\Sigma}) = P(\boldsymbol{x}|\boldsymbol{\Delta}, \boldsymbol{\Sigma})$. We can calculate the likelihood of the measured time series belonging to each distribution using the translated distributions and get the same result.

To derive an expression of F_1 score specific to our model, we start from the definition

$$F_1 = \frac{2TP}{2TP + FN + FP} \tag{13}$$

where 'TP' is the true positive rate, 'FP' is the false positive rate, and 'FN' is the false negative rate. Let $\boldsymbol{\Delta}$ be the positive label and $\boldsymbol{0}$ be the negative label. Then, we can define true positive rate as, the probability of assigning a positive label to a sample that belongs to the positive distribution $\boldsymbol{\mathcal{N}}(\boldsymbol{\Delta}, \boldsymbol{\Sigma})$. As illustrated in Fig. 5, all samples that belong to $\boldsymbol{\mathcal{N}}(\boldsymbol{\Delta}, \boldsymbol{\Sigma})$ and fall on the right side of the decision boundary, in other words, closer to the $\boldsymbol{\mathcal{N}}(\boldsymbol{\Delta}, \boldsymbol{\Sigma})$ distribution, will be correctly labeled positive. This proximity, as we will elaborate later, can be measured using the Mahalanobis Distance (De Maesschalck et al. 2000).

We define the mathematical expression for true positive rate, false negative rate, true negative rate, and false positive rate as follows,

$$\begin{aligned}
TP &= P\Big[P(\boldsymbol{x}|\boldsymbol{0}, \boldsymbol{\Sigma}) < P(\boldsymbol{x}|\boldsymbol{\Delta}, \boldsymbol{\Sigma}) \Big| \boldsymbol{x} \sim \boldsymbol{\mathcal{N}}(\boldsymbol{\Delta}, \boldsymbol{\Sigma})\Big] \\
FN &= P\Big[P(\boldsymbol{x}|\boldsymbol{0}, \boldsymbol{\Sigma}) > P(\boldsymbol{x}|\boldsymbol{\Delta}, \boldsymbol{\Sigma}) \Big| \boldsymbol{x} \sim \boldsymbol{\mathcal{N}}(\boldsymbol{\Delta}, \boldsymbol{\Sigma})\Big] \\
TN &= P\Big[P(\boldsymbol{x}|\boldsymbol{0}, \boldsymbol{\Sigma}) > P(\boldsymbol{x}|\boldsymbol{\Delta}, \boldsymbol{\Sigma}) \Big| \boldsymbol{x} \sim \boldsymbol{\mathcal{N}}(\boldsymbol{0}, \boldsymbol{\Sigma})\Big] \\
FP &= P\Big[P(\boldsymbol{x}|\boldsymbol{0}, \boldsymbol{\Sigma}) < P(\boldsymbol{x}|\boldsymbol{\Delta}, \boldsymbol{\Sigma}) \Big| \boldsymbol{x} \sim \boldsymbol{\mathcal{N}}(\boldsymbol{0}, \boldsymbol{\Sigma})\Big]
\end{aligned} \tag{14}$$

Note, the two distributions $\boldsymbol{\mathcal{N}}(\boldsymbol{0}, \boldsymbol{\Sigma})$ and $\boldsymbol{\mathcal{N}}(\boldsymbol{\Delta}, \boldsymbol{\Sigma})$ have identical spherical covariance matrix, so we have $TP = TN$, and $FN = FP$. Therefore, the expression for F_1 score can be simplified as follows

$$\begin{aligned}
F_1 &= \frac{2TP}{2TP + FN + FP} \\
&= \frac{TP}{TP + FN} \\
&= TP/1 = 1 - FP
\end{aligned} \tag{15}$$

Now we derive the expression for FP, where we assume $\boldsymbol{x} \sim \boldsymbol{\mathcal{N}}(\boldsymbol{0}, \boldsymbol{\Sigma})$

$$FP = P\Big[P(\boldsymbol{x}|\boldsymbol{0}, \boldsymbol{\Sigma}) < P(\boldsymbol{x}|\boldsymbol{\Delta}, \boldsymbol{\Sigma})\Big] \tag{16}$$

Using the Square of Mahalanobis distance, which is proportional to the negative log-likelihood (De Maesschalck et al. 2000), we have

$$
\begin{aligned}
FP &= P\Big[(\boldsymbol{x}-\mathbf{0})^T\boldsymbol{\Sigma}^{-1}(\boldsymbol{x}-\mathbf{0}) > (\boldsymbol{x}-\boldsymbol{\Delta})^T\boldsymbol{\Sigma}^{-1}(\boldsymbol{x}-\boldsymbol{\Delta})\Big] \\
&= P\Big[\sum_{i=1}^{n} x_i^2 \Big/ \sigma^2 > \sum_{i=1}^{n}(x_i-\Delta_i)^2 \Big/ \sigma^2\Big] \\
&= P\left[\frac{\sum_{i=1}^{n}(x_i-\Delta_i)^2 \Big/ \sigma^2}{\sum_{i=1}^{n} x_i^2 \Big/ \sigma^2} < 1\right]
\end{aligned} \tag{17}
$$

Let $X = \sum_{i=1}^{n}(x_i-\Delta_i)^2 \Big/ \sigma^2$, $Y = \sum_{i=1}^{n} x_i^2 \Big/ \sigma^2$, and $F = (Y/n)/(X/n)$, we have

$$
FP = P\left[\frac{X}{Y} < 1\right] = P\left[\frac{X/n}{Y/n} < 1\right] = P(F<1) \tag{18}
$$

Note that $x_i \sim i.i.d.\mathcal{N}\left(0,\sigma^2\right)$ and $(x_i-\Delta_i) \sim i.i.d.\mathcal{N}\left(-\Delta_i,\sigma^2\right)$. It follows that X is a noncentral chi-squared random variable with n degrees of freedom and noncentrality parameter $\lambda = \sum_{i=1}^{n}\Delta_i^2 \Big/ \sigma^2$. Y is a central chi-squared random variable with n degrees of freedom. As a result, random variable F falls under a noncentral F-distribution. Then, we can calculate $P(F<1)$ by evaluating the cumulative distribution function of F, which we will refer as CDF_F, at 1 (Johnson 1972). We used the implementation from Pav (2017) in 'R' language to calculate $CDF_F(1)$.

The expression for F_1 score is

$$
\begin{aligned}
F_1 &= 1 - FP = 1 - CDF_F(1) \\
F_1 &= 1 - \sum_{j=0}^{\infty}\left(\frac{(\frac{1}{2}\lambda)^2}{j!}e^{-\frac{\lambda}{2}}\right) I\left(\frac{1}{2}\middle|\frac{n}{2}+j,\frac{n}{2}\right) \\
where\ \lambda &= \frac{1}{\sigma^2}||\boldsymbol{\Delta}||_2^2 = \frac{1}{\sigma^2}\sum_{i=1}^{n}\Delta_i^2
\end{aligned} \tag{19}
$$

λ is the noncentrality parameter, I is the regularized incomplete beta function (Patnaik 1949), and

$$
\Delta_i = (T_{surf1} - T_{surf2}) * erfc\left(\frac{x}{2\sqrt{\alpha_{sens}t_i}}\right) \tag{20}
$$

where T_{surf1} and T_{surf2} can be calculated by Eq. 1. Thus, we have

$$
\begin{aligned}
\lambda &= \frac{1}{\sigma^2}\sum_{i=1}^{n}\left(T_{surf1}-T_{surf2}\right)^2 * erfc^2\left(\frac{x}{2\sqrt{\alpha_{sens}t_i}}\right) \\
&= \frac{\left(T_{surf1}-T_{surf2}\right)^2}{\sigma^2}\sum_{i=1}^{n} erfc^2\left(\frac{x}{2\sqrt{\alpha_{sens}t_i}}\right)
\end{aligned} \tag{21}
$$

Let $\Delta t = t_{i+1} - t_i$ represent the sample time. We have,

$$
\lambda = \frac{\left(T_{surf1}-T_{surf2}\right)^2}{\sigma^2 * \Delta t}\sum_{i=1}^{n} erfc^2\left(\frac{x}{2\sqrt{\alpha_{sens}t_i}}\right) * \Delta t \tag{22}
$$

We assume that sample time Δt is small so that $\sum_{i=1}^{n} erfc^2\left(\frac{x}{2\sqrt{\alpha_{sens}t_i}}\right) * \Delta t$ can be approximated with $\int_0^{t_{contact}} erfc^2\left(\frac{x}{2\sqrt{\alpha_{sens}t}}\right) dt$.

Therefore, the resulting final expression for F_1 score is given by,

$$
\begin{aligned}
F_1 &= 1 - \sum_{j=0}^{\infty}\left(\frac{(\frac{1}{2}\lambda)^2}{j!}e^{-\frac{\lambda}{2}}\right) I\left(\frac{1}{2}\middle|\frac{n}{2}+j,\frac{n}{2}\right) \\
where\quad \lambda &= \frac{\left(T_{surf1}-T_{surf2}\right)^2}{\sigma^2 * \Delta t} \\
&\quad * \int_0^{t_{contact}} erfc^2\left(\frac{x}{2\sqrt{\alpha_{sens}t}}\right) dt
\end{aligned} \tag{23}
$$

6 EVALUATIONS OF PERFORMANCE MODEL

We evaluate our performance model using a three-part evaluation. First, we focus on classifying two different thermal effusivities. We compare the prediction of our performance model with the performance of SVM in classifying simulated sensor time-series data for two different thermal effusivities. We use SVM because it is a widely used data-driven algorithm and we have previously achieved success with SVM for material recognition tasks using active thermal sensing (Bhattacharjee et al. 2016, 2015). We use a wide range of thermal effusivities to compare the performance and analyze the effect of noise and sensor initial condition on the performance.

Second, we focus on binary material recognition for all materials in the CES-Edupack Level 1 Database (Ashby 2008). We compare the prediction of the performance model with that of SVM in binary material recognition tasks for simulated time-series heat transfer data. We simulate data using consistent sensor initial conditions.

Third, we focus on binary material recognition of 12 real-world materials. We compare the prediction of the performance model in binary material recognition tasks for real-world time-series heat transfer data collected using a 1-DoF robot from 12 different materials under both consistent and varied sensor initial conditions.

We use F_1 scores as a metric to compare the performances for all three cases. Figure 7 shows a schematic of the evaluation method.

7 EVALUATIONS WITH DIFFERENT THERMAL EFFUSIVITIES

In this section, we evaluate our performance model by comparing its F_1 score for classifying two different thermal effusivities with the F_1 score obtained with SVM and simulated time-series data. We used SVM as our data-driven

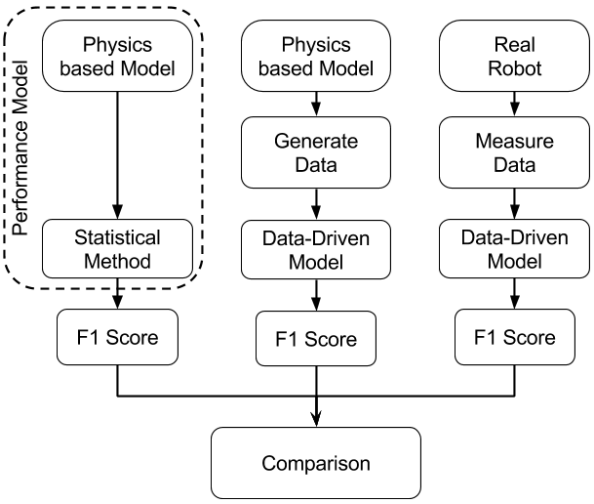

Figure 7. *Evaluation of our Performance Model.*

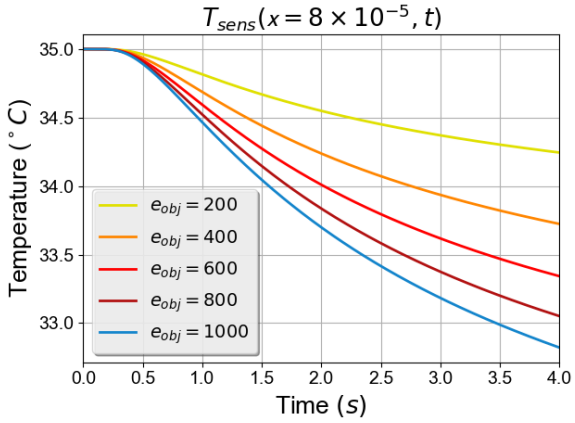

Figure 8. *Examples of generated time-series heat transfer data from our physics-based model for some example effusivity values.*

method given its best performance in our previous work (Bhattacharjee et al. 2015, 2016).

Given a reference thermal effusivity value, we are interested in comparing the performance model result and the SVM result for the minimum effusivity difference required to obtain a binary classification F_1 score greater than or equal to a desired performance (Φ). In this paper, we set $\Phi = 0.9$. This means we consider any effusivity pair with $F_1 \geq 0.9$ classification score as distinguishable.

7.1 Minimum Distinguishable Difference $\delta(e)$

For a given thermal effusivity value e, let $\delta(e)$ be the smallest value such that either $F_1(e, e + \delta(e))$ or $F_1(e, e - \delta(e))$ is greater than Φ. We then define the minimum distinguishable difference of the given effusivity value e to be $\delta(e)$. Intuitively, $\delta(e)$ for a given e provides us with a quantitative evaluation of what materials can be distinguished from a specific material with effusivity e under the current sensor, material and environmental conditions.

7.2 Evaluation Procedure

When a thermal sensor comes in contact with a material sample, the heat transfer data are affected by sensor noise, initial sensor temperature as well as the contact duration. Therefore, we analyze the effect of these parameters on the F_1 score obtained with our model as well as with SVM by varying the quantities as given below:

- Noise $Z \sim \mathcal{N}\left(0, \sigma^2\right)$: $\sigma = 0.01$, $\sigma = 0.05$ and $\sigma = 0.10$
- Initial Sensor Temperature $T_{sens}(t = 0)$: 30°C and 35°C
- Contact Duration $t_{contact}$: 1.00s, 2.00s, 3.00s, and 4.00s

We estimated the minimum distinguishable difference $\delta(e)$ for every effusivity value e for the above conditions with the model and with SVM and compared the results. For our performance model, we used the statistical method to calculate the F_1 score under the given sensor and material thermal properties using Eq. 23. For SVM, we generated noisy data using the physics-based model and performed a 3-fold cross-validation over each unique effusivity value pair and reported the F_1 score.

We used the implementation of binary support vector machine (SVM) provided by the scikit-learn package (Pedregosa et al. 2011) in Python. We used the linear kernel for the classification task. To produce feature vectors for training, we used both raw temperature and estimated local slope from each trial of the experiment, and concatenated them into a single feature vector.

7.3 Data Collection

In order to account for a sufficiently large thermal effusivity range, we referred to the CES EduPack 2016 (Granta Design Ltd., Cambridge, UK 2016) Level 1 material database. Of all the included materials, Rigid Polymer Foam (LD) has the minimum effusivity value of $3.05 \times 10^1 J/(s^{\frac{1}{2}} \cdot K \cdot m^2)$, and Copper Alloy has the maximum effusivity value of $3.68 \times 10^4 J/(s^{\frac{1}{2}} \cdot K \cdot m^2)$. Therefore, we sampled effusivity values in the range $(0, 4.00 \times 10^4]$ $J/(s^{\frac{1}{2}} \cdot K \cdot m^2)$. We discretized the range to 500 equal intervals. We can think of each interval as a material category, and an instance of the material category can take on any effusivity value within the interval.

Given an effusivity value e, we constructed the time series heat transfer data based on the semi-infinite solid model defined in Section 4.1. We use $e_{sens} = 892$ $(J \cdot s^{-\frac{1}{2}} \cdot K^{-1} \cdot m^{-2})$, and $\alpha_{sens} = 1.19 \times 10^{-9}$ $(m^2 \cdot s^{-1})$ similar to our real-world sensor parameters (See Appendix A). Note our real-world sensor noise was $\sigma = 0.05$. We set T_{amb} to 25°C. We set the sampling rate to be 200 Hz, similar to our real-world sensor sampling rate. Figure 8 shows examples of data generated using our physics-based model with these parameters and some example object effusivity values.

We generated 50 trials for each effusivity interval by uniformly sampling from the effusivity interval and generated simulated data with the sampled effusivity. We performed all simulations using a 2015 MacBook Pro equipped with Intel Core i7 CPU at 3.1 GHz running OS X El Capitan Version 10.11.6.

7.4 Results and Discussion

In this section, we present and compare the results of our performance model and SVM. Figure 9 shows the F_1 score Matrix with pairwise F_1 scores for all effusivity values using our performance model and SVM. We obtained this matrix using $t_{contact} = 2s$, $T_{sens}(t = 0)$ = 35°C, and $\sigma = 0.05$. Table 1 shows the percentage of indistinguishable effusivity combinations calculated based on the F_1 score matrices with $\Phi = 0.9$. The results show that the evaluation using our performance model matches well with the evaluation using SVM.

Table 1. Percentage of Indistinguishable Effusivity Combinations, $t_{contact} = 2.00s$

Experimental Conditions		Performance Model		SVM	
		Temperature Difference		Temperature Difference	
		5°C	10°C	5°C	10°C
Noise	0.10	62.97%	45.96%	55.54%	38.61%
	0.05	45.96%	30.00%	38.62%	24.41%
	0.01	14.69%	7.89%	23.30%	13.26%

We compared the F_1 score matrices predicted by the performance model and SVM by calculating the L_1 distance between the two matrices. Before we calculated the L_1 distance, we converted the F_1 score matrix into a binary map where any score greater than 0.9 (our threshold for determining whether a material is distinguishable) is converted to 1 and the any score less than 0.9 is converted to 0. The L_1 distance (Crowley and Krause 1988) between two $n \times n$ converted matrices $\mathbf{A}$ and $\mathbf{B}$ is defined as:

$$||\mathbf{A} - \mathbf{B}||_1 = \sum_{i=1}^{n} \sum_{j=1}^{n} |a_{ij} - b_{ij}| \tag{24}$$

Since the F_1 score matrix is symmetrical, and the diagonal values in the matrix are trivial (a material's recognition performance with itself is not meaningful), we only consider the upper diagonal matrix in the following accuracy metric,

$$d(\mathbf{A}, \mathbf{B}) = \left(1 - \sum_{i=1}^{n-1} \sum_{j=i+1}^{n} |a_{ij} - b_{ij}| \times \frac{2}{n(n-1)}\right) \times 100\% \tag{25}$$

This gives a measure of the difference between two F_1 score matrices. We used this metric to compare the difference between our performance model F_1 score matrix and the F_1 score matrix obtained with SVM running on both simulated and experimental data. Table 2 shows that the F_1 score matrices predicted by our performance model match well with the F_1 score matrices produced by SVM.

In order to capture the impact of initial condition $T_{sens}(t = 0)$ and noise Z, we calculated minimum distinguishable difference $\delta(e)$ for all values of e for each of the conditions. Figures 10 and 11 show the results.

7.4.1 Effect of Contact Duration

To analyze the effect of contact duration on classification performance, we truncated the time series data at different time lengths and ran our performance model and SVM on the truncated data. Fig. 10 shows the minimum distinguishable difference $\delta(e)$ curves calculated based on the performance model results (left graphs). As expected, in each plot, with increased length of time, the material recognition performance of the algorithm improves. Figure 10 also shows the results from SVM, and it follows the same trend (right graphs). The more the contact duration, the better is the performance of material recognition (See Section 10).

Table 2. Percent Matching Between Performance Model Predictions and SVM Results of Indistinguishable Effusivity Combinations, $t_{contact} = 2.00s$

Experimental Conditions		Temperature Difference	
		5°C	10°C
Noise	0.10	92.60%	92.65%
	0.05	92.63%	94.38%
	0.01	91.45%	94.65%

7.4.2 Effect of Initial Condition

Figure 10 shows the results with our performance model (left-graphs) and SVM (right-graphs) for both $T_{sens}(t = 0) = 30$°C and $T_{sens}(t = 0) = 35$°C initial conditions. By comparing the ($T_{sens}(t = 0) = 35$°C) graphs with the ($T_{sens}(t = 0) = 30$°C) graphs in Fig. 10, we observe that larger initial temperature difference ($T_{sens}(t = 0) = 35°C$) between sensor and ambient environment produces a lower $\delta(e)$ curve. In other words, our model predicts that a larger initial temperature difference between sensor and measured object can help in material recognition, as it generates more distinguishable heat transfer data for materials (See Section 10).

Also, the graphs generated by the performance model are visually similar to the ones generated by SVM across different initial sensor temperature conditions. Observe that SVM actually performs slightly better than the performance model for each specified $t_{contact}$, with $\delta(e)$ curves just below that of the performance model. This is probably because SVM are less susceptible to the additive Gaussian noise in the data than the performance model.

7.4.3 Effect of Noise

Figure 11 shows the results with our performance model (top graphs) and SVM (bottom graphs) for different levels of noise. By comparing the left plot ($\sigma = 0.01$) with the middle plot ($\sigma = 0.05$) and the right plot ($\sigma = 0.10$) in Fig. 11, we observe the impact of noise on the algorithm performance. As expected, simulations with a noise level $\sigma = 0.10$ produce the highest $\delta(e)$ values. Again, our models predict that thermal sensors with lower noise help in material recognition (See Section 10) and the graphs generated by our performance model are similar to the ones generated by SVM.

8 EVALUATIONS WITH SIMULATED DATA FROM A MATERIAL DATABASE

In this set of experiments, we mapped the previous results obtained using different thermal effusivity values to actual material effusivity values. Our objective here is to evaluate our performance model using actual material effusivity values. We obtained thermal effusivity values of all 69 materials from CES EduPack Level 1 database (Ashby

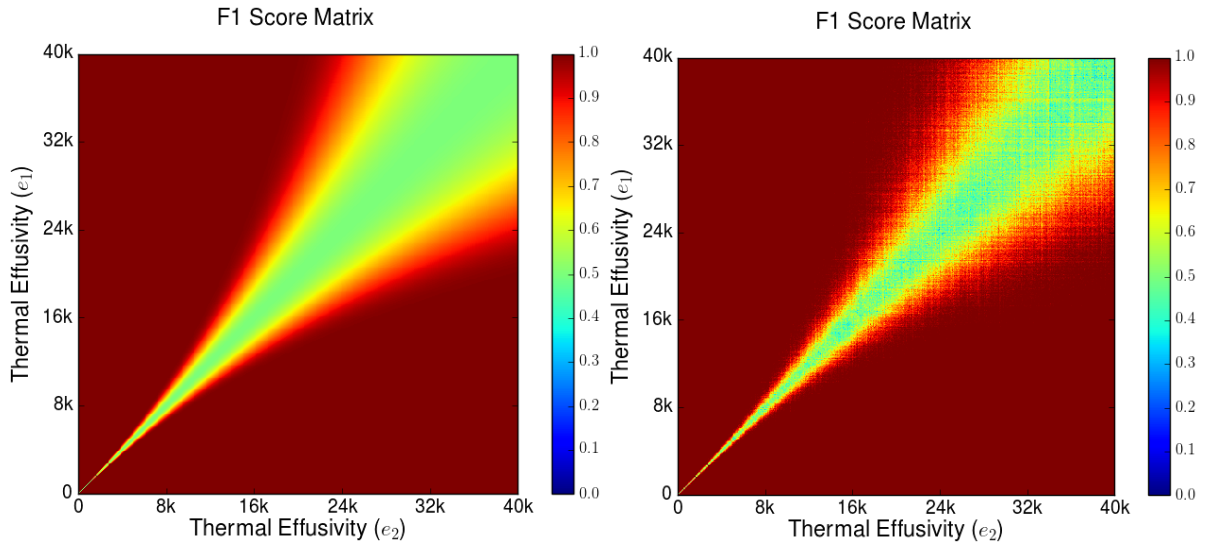

Figure 9. *Example F_1 score Matrix with our performance model (left) and SVM (right) (T_{sens} = 35°C, σ = 0.05, $t_{contact}$ = 2.00s)*

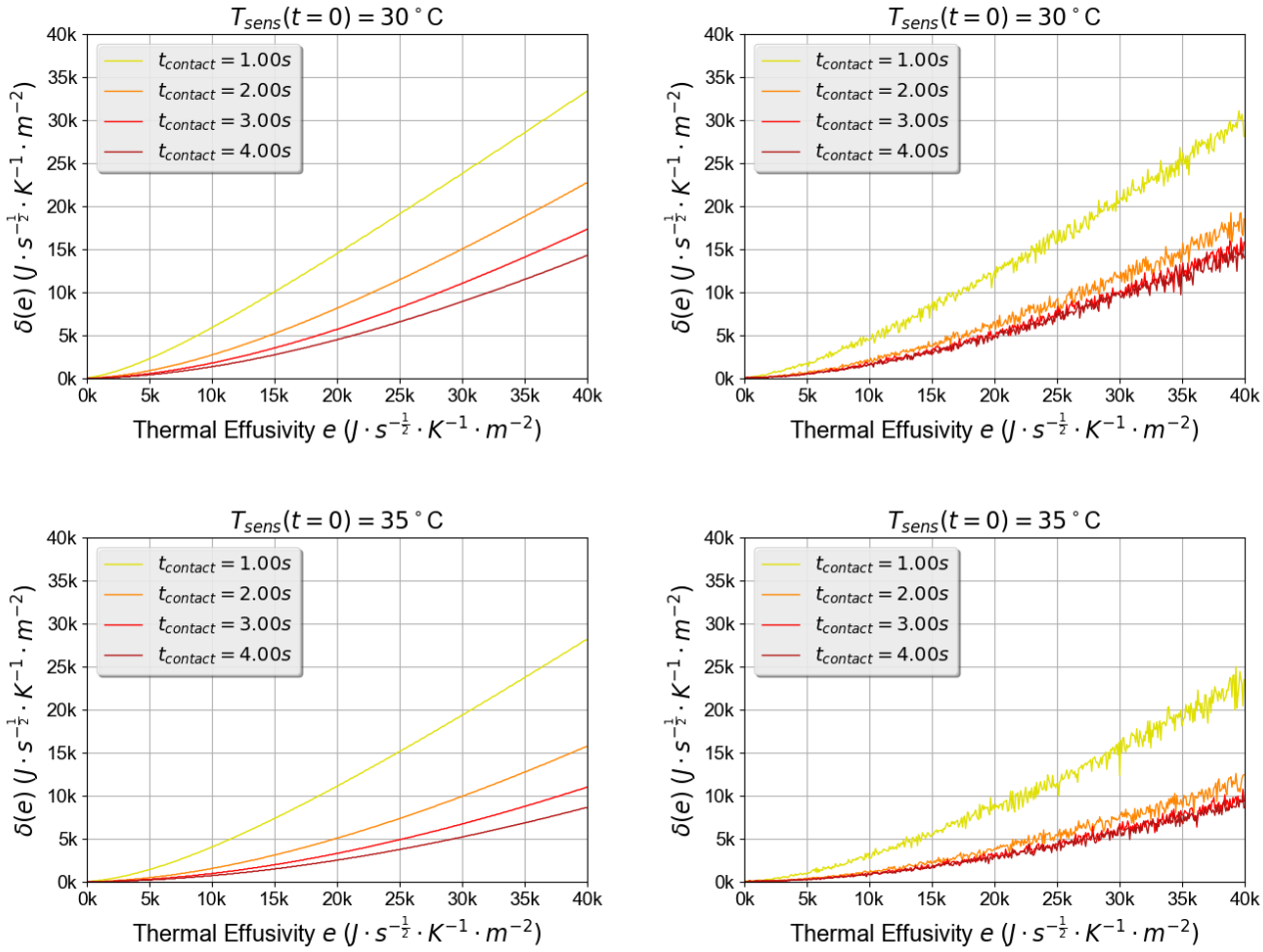

Figure 10. *Effect of Initial Condition on $\delta(e)$ with fixed noise $\sigma = 0.05$: Performance Model and $T_{sens}(t=0)$ = 30° C (Top-left), SVM and $T_{sens}(t=0)$ = 30° C (Top-Right), Performance Model and $T_{sens}(t=0)$ = 35° C (Bottom-left), and SVM and $T_{sens}(t=0)$ = 35° C (Bottom-Right)*

2008). Figure 12 shows the effusivity ranges of all the 69 materials. We looked up binary material classification results for all possible pairs of effusivity values corresponding to 69 materials (2346 material pairs) from our previous results in Section 7.4 to find out what materials are distinguishable with F_1 score greater than $\Phi = 0.9$. We compared the results of our performance model with that of SVM. We present the F_1 score matrices in terms of node graphs of distinguishable and indistinguishable pairs.

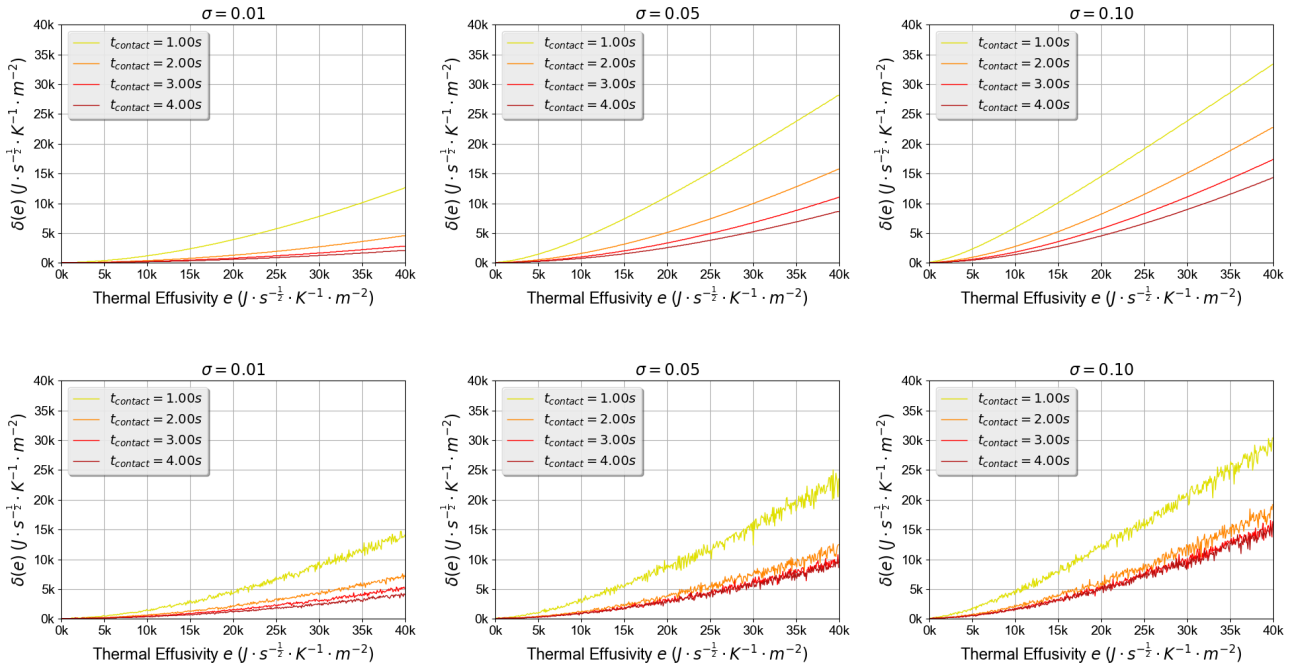

Figure 11. *Effect of Noise on $\delta(e)$ with fixed initial condition $T_{sens}(t = 0) = 35°C$: Top graphs show the results from the performance model whereas the bottom graphs show the results from SVM. The noise levels increase from ($\sigma = 0.01$) in the left graphs to ($\sigma = 0.05$) in the middle graphs, and finally ($\sigma = 0.1$) in the right graphs.*

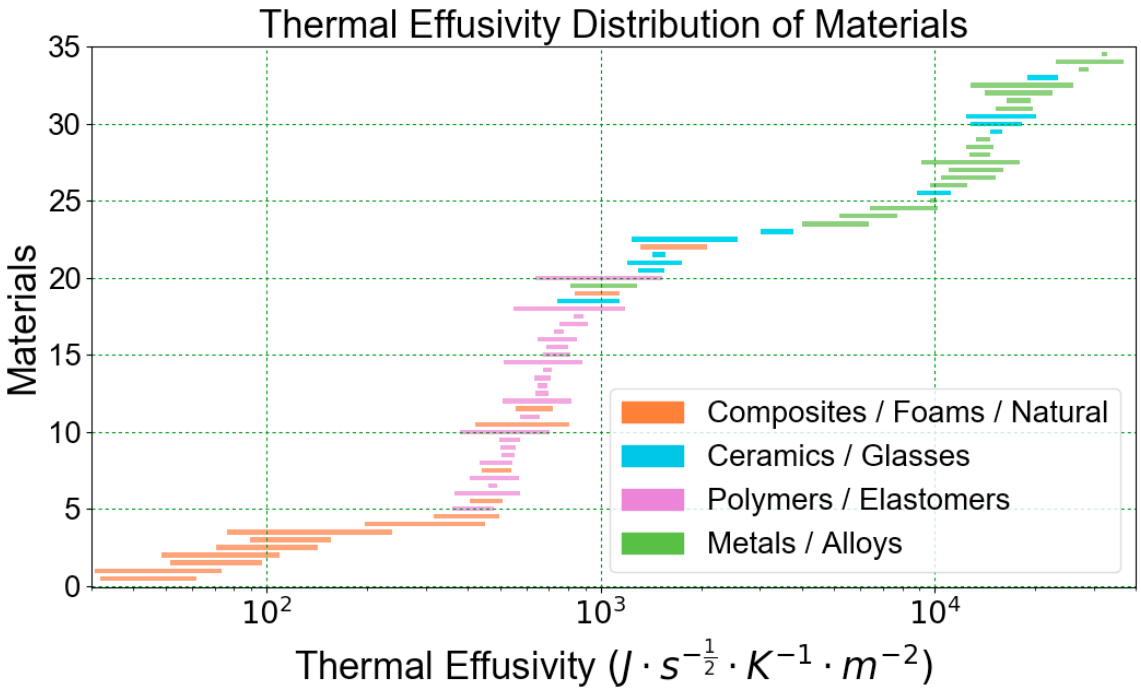

Figure 12. *Effusivity Distribution of the 69 Materials in CES Edupack Level 1 (Ashby 2008) in Logarithmic Scale*

8.1 Node Graphs of Material Pairs

To visualize whether any two materials from the CES EduPack Level 1 database (Ashby 2008) are distinguishable, we generated a node-graph based on their F_1 scores where each node represents a material. The node-graph has the following characteristics:

- An edge between two material nodes represents that they are indistinguishable. Note $\Phi = 0.9$.
- The radius of a material node is proportional to its thermal effusivity. So, metals with larger effusivities are represented by larger circles.
- CES Edupack divides all materials into four large categories such as metals/alloys, ceramics/glasses, polymers/elastomers, and composites/foams/natural. A material node's color signifies which category the material belongs to.
- The thickness of the edge connecting two materials is inversely proportional to their F_1 score. This means

that the thicker the edge, the more difficult it is to distinguish the material nodes that are at its ends.
- The relative position of the nodes has no relation with any physical property. It is purely for visualization purposes.

Note, each material in the CES Edupack database (Ashby 2008) has a range of thermal effusivity values that it can have. So, to calculate a single F_1 score for the range of effusivity values for a single material pair, we used the average F_1 score ≥ 0.9. To find the average F_1 score, for example, for gold and silver, we find the average of F_1 scores for the binary classification between all possible combinations of gold effusivities and silver effusivities. In our case, the average F_1 score can be calculated based on the F_1 score matrix, as shown in Fig. 9, by taking the average of all F_1 scores within a rectangular area, bounded by effusivity values ($e1$) in the effusivity range of the first material (gold), and effusivity values ($e2$) in the effusivity range of the other (silver).

Figure 13 shows the results with $T_{sens}(t = 0) = 35°\text{C}$ and $N = 0.05$ noise. We see that the results with our performance model match well with the results with SVM. From the figure, we note that there are three to four connected components in each node-graph and these connected components tend to have the majority of the material nodes in a particular category such as metals/alloys, ceramics/glasses, polymers/elastomers, and composites/foams/natural. This further means that a material belonging to one of these categories has a higher probability of being distinguished from a material in another category than in its own category. For example, it would be easier to distinguish a ceramic from a metal than another ceramic. We can also see some densely connected components in the graph. For example, metals are densely connected together, which agrees with our observation in Fig. 10, as rising $\delta(e)$ makes it harder to distinguish materials with larger effusivity.

The observed connected components also agree well when compared with the effusivity ranges provided in Fig. 12. Metals, with large effusivity values, are generally difficult to distinguish amongst themselves because their effusivity values are so large that they dominate T_{surf} (Eq.1) to a value very close to the ambient temperature, rendering the T_{sens} curves indistinguishable.

While our performance model predicts better $\delta(e)$ for smaller effusivity values, polymers/elastomers and composites/foams/natural materials still form many edges, because the effusivity values of materials are so close that their difference is smaller than the minimum distinguishable distance $\delta(e)$.

Table 3. Percentage of Indistinguishable Pairs, $t_{contact} = 2.00s$

Experimental Conditions		Performance Model		SVM	
		Temperature Difference		Temperature Difference	
		5°C	10°C	5°C	10°C
Noise	0.10	22.42%	14.54%	21.14%	15.77%
	0.05	14.54%	10.61%	14.96%	12.53%
	0.01	7.08%	5.16%	11.94%	8.35%

As shown in Table 3, the number of edges present in the graph is consistent with the observation we made in Fig. 10, which means that a larger initial temperature difference between the sensor and the material and less noise lead to more distinguishable material pairs. Also, the quantitative values using the performance model match well with that of SVM. As shown in Table 4 the indistinguishable material pairs predicted by our performance model match with the SVM results with around 96% accuracy across all experimental conditions.

Table 4. Percent Matching Between Performance Model Predictions and SVM Results of Indistinguishable Material Pairs, $t_{contact} = 2.00s$

Experimental Conditions		Temperature Difference	
		5°C	10°C
Noise	0.10	98.55%	96.63%
	0.05	97.53%	96.63%
	0.01	95.14%	96.80%

9 EVALUATIONS WITH A REAL ROBOT

9.1 Experimental Setup

Figure 1 shows the 1-DoF robot used in our experiments. The robot consists of a linear actuator, two Teensy 3.2 microcontrollers, a passive sensing thermistor, and an active sensing module. The active sensing module consists of the Thorlabs HT10K Flexible Polyimide Foil Heater with 10 kOhm Thermistor (tho 2016) (heating element and a temperature sensor) on a fabric-based force sensor (Bhattacharjee et al. 2013) which is backed by thermal insulation foam. The passive sensing thermistor uses the fast-response $10k\Omega$ NTC thermistor (EPCOS B57541G1103F) (epc 2016).

Figure 15 shows the list of materials used for this set of experiments. We selected these materials in order to have a uniform representation of materials from all the four categories (metals, ceramics, polymers, and composites) from the CES Edupack database (Ashby 2008). We included 3 materials from each category. We selected 12 materials such that it has both distinguishable and indistinguishable material pairs between them. We estimated this by running our performance model using the mid-point of the effusivity range of these materials.

9.2 Experimental Procedure

Figure 1 shows an example of the 1-DoF robot reaching to touch a cardboard sample. We used a Python script on a separate Dell Optiplex 9010 Computer equipped with Intel(R) Core(TM) i7-3770 CPU at 3.40GHz running 32-bit Ubuntu 12.04.2 LTS system with Linux Ubuntu 3.5.0-54-generic kernel to control the device through a serial link with the Teensy 3.2 microcontrollers. Before reaching down and contacting the sample, the device waits at 15 mm above the sample, to allow a voltage supply to generate heat based on an integral controller such that the active sensing thermistor maintains the desired temperature. Upon contact with the material sample, the integral controller stops so as not to interfere with the natural heat transfer from the sensor to the material sample. The micro-controllers record the active sensing thermistor and the passive sensing thermistor

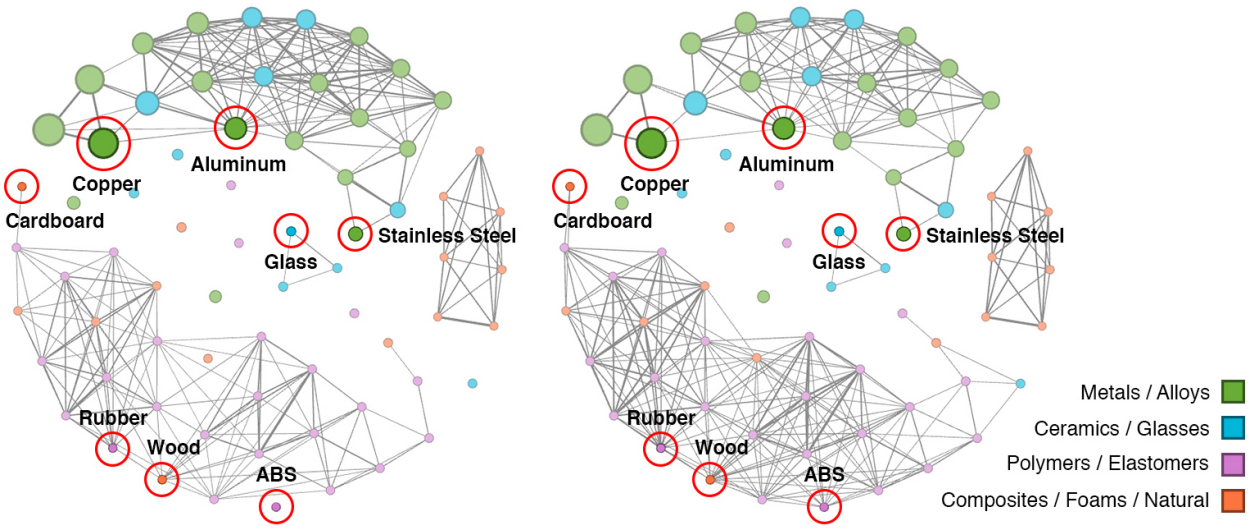

Figure 13. *Node Graphs of Material Pairs using Performance Model (left) and SVM (right)*

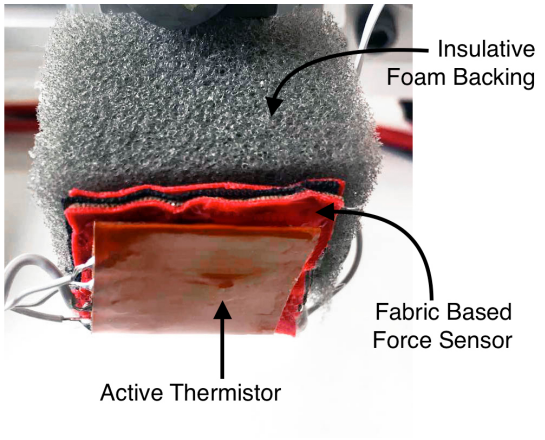

Figure 14. *The sensing module with fabric-based force sensor and an active thermal sensor*

Figure 15. *Twelve selected materials for real-world experiments with the 1-DoF robot*

readings at 200 Hz for 10 seconds. Note, the sensor has an insulated foam backing which makes the sensor compliant and thus, to ensure that there is complete contact between the material sample and the sensor's flat surface, we use a force threshold of 5 N to detect the onset of contact. Also, we do not use the passive thermistor data for any material recognition purposes. The robot then raises the sensing module and waits for 20 seconds before starting the next trial. Using the FLIR Tau 2 324 7.5mm Thermal Imaging Camera Core (46324007H-FRNLX), we found that 20 seconds were enough for the material samples to come back to their initial state. This is to ensure that the sample is at a consistent initial condition before the robot touches it at any trial (see Extension 1).

We performed two sets of experiments with the real robot. The first set consisted of 10 trials each with fixed initial sensor temperature conditions for each material. The second set consisted of 50 trials each with uniformly varied initial sensor temperature conditions for each material. We uniformly varied the initial sensor conditions between $T_{sens}(t = 0) = 30°\text{C}$ to $T_{sens}(t = 0) = 35°\text{C}$. We identified the sensor and material parameters as outlined in Appendix 12. We performed this set of experiments to simulate contact situations when a robot incidentally touches objects in its environment without the opportunity to adjust its initial sensor conditions. This is a common scenario in manipulation in cluttered and unstructured environments or in assistive scenarios working in close contact with a human body (Bhattacharjee et al. 2014).

9.3 Results

9.3.1 Fixed Initial Conditions With fixed initial conditions, SVM achieved an average F_1 score of 0.985 for binary material recognition across all 66 material pair comparisons. Our performance model result successfully achieved a 92.42% match with the SVM results, using the metric defined in Eq. (25). While the performance model predicted that MDF vs. Acrylic can only be distinguished with 0.62 F_1 score, SVM were able to achieve an F_1 score of 0.92.

9.3.2 Varied Initial Conditions In order to test the accuracy of the performance model under varied initial conditions, we collected 50 trials of data for each material

with varied sensor initial conditions by uniformly sampling $T_{sens}(t=0)$ from 30°C to 35°C before contact. SVM achieved an average F_1 score of 0.976 for binary material recognition across all 66 material pair comparisons.

However, for variable initial conditions, the expected resulting distribution is a high dimensional "plateau" shaped multivariate generalized normal distribution (Nadarajah 2005), which our statistical method cannot directly account for. To apply our performance model to trials collected with varied initial conditions, we need to transform the data to fixed initial conditions. We achieved this by transforming the data as follows.

By using Eq. (5) and substituting T_{surf} with Eq. (2), we have the following relation,

$$\begin{aligned} &\frac{T_{sens}(x,t) - T_{obj}(t=0)}{T_{sens}(t=0) - T_{obj}(t=0)} = \\ &1 - \frac{e_{obj}}{e_{obj}+e_{sens}} erfc\left(\frac{x}{2\sqrt{\alpha_{sens} t}}\right) \\ &+ \frac{Z \sim \mathcal{N}\left(0, \sigma^2\right)}{T_{sens}(t=0) - T_{obj}(t=0)} \end{aligned} \tag{26}$$

where all initial conditions are transformed to 1, and the expected noise level Z' of the transformed data becomes,

$$\begin{aligned} Z' &= \frac{1}{35-30} * \int_{T\in[30,35]} \frac{Z}{T - T_{obj}(t=0)} dT \\ &= \frac{ln35 - ln30}{35-30} * Z \end{aligned} \tag{27}$$

Using the above transformation, our performance model prediction successfully achieved a 90.91% match with the real-world data performance obtained with SVM. The performance model successfully predicted the majority of distinguishable material pairs. It also successfully predicted that ABS and Rubber, and MDF and Rubber would be indistinguishable under the given sensor and environmental conditions. Interestingly, our performance model predicted that Copper vs. Aluminum would be indistinguishable, but SVM could distinguish them. Out of the four pairs of materials (ABS vs. MDF, Copper vs. Stainless Steel, ABS vs. Wood, and Aluminum vs. Stainless Steel) that the performance model expected to distinguish, SVM achieved F_1 score ≤ 0.9, but managed to achieve an average F_1 score of 0.83.

10 LIMITATIONS

Note, the model does not explicitly model contact area but heat transfer depends on contact area. For example, in this paper, we used the active thermal sensor similar to the one used in Bhattacharjee et al. (2015). However, we also performed all these three evaluations with another 'point' thermal sensor used in Wade et al. (2016). We call the sensor a 'point' sensor because it is a thermistor of small cross-sectional area. For experiments with fixed initial conditions, our model predicted the performance well using the point sensor. The model performance matched the SVM performance with 92.29% accuracy using the metric (See Eq.25) for effusivity combinations, 99.94% for simulated data from the material database, and 86.36% for real-world data with fixed initial conditions. However, the model predictions matched the real-world data with varied initial conditions with only 46.97% accuracy for the 'point' sensor. Basically, the model predicted that a lot of the binary material pairs are distinguishable but the SVM running on the real-world data collected using the 'point' sensor could distinguish only 22 out of the 66 material pairs. This is probably because the sensor is a 'point' sensor whose contact area during heat transfer is low. Thus, the difference in the heat transfer between materials is less prominent than the 'flat area' sensor used in this paper and Bhattacharjee et al. (2015). This relates to the fact that heat transfer is dependent on the contact area and geometry as well how well two surfaces are in contact. Thus, depending upon the compliance in the sensor, application of larger force might result in a better contact area or contact between two flat surfaces may result in more prominent heat transfer than contact between a flat surface and a spherical surface ('point' sensor) or between two spherical surfaces. This is compounded by the fact that the point sensors were also in contact with the fabric, thus adding more uncertainty to the heat transfer data. Also, the 'point' sensor parameters may be more susceptible to temperature changes, i.e., the thermal effusivity and diffusivity of the 'point' sensor may have changed significantly with temperature changes in the sensor. Thus, during varied initial conditions, the heat transfer data were more unpredictable than obtained using a fixed sensor initial condition in our physics-based model. Accounting for the sensor parameter dependence on temperature, the effect of the contact area, as well the force applied during physical contact, in the heat transfer data using the semi-infinite model needs further investigation.

11 DISCUSSION

The physics-based analytical performance model in this paper could be used to design thermal sensors to achieve a desired level of performance and to provide various experimental design guidelines based on its predictions. For example, if our goal is for a robot with a thermal sensor to achieve approximately 90% F_1 score with all the 69 materials in the CES Edupack Level 1 database, our model suggests that the thermal sensor initial temperature should be at least 10°C than the material initial temperature and the temperature sensor should at most have a noise of 0.05°C (See Table 3). Another example is, if our robot has an accurate thermal sensor with noise 0.01°C, our model suggests that the sensor can achieve greater than 90% F_1 score even when the sensor initial temperature is just 5°C higher than the material initial temperature, thus reducing the power requirements (See Table 3). To give one final example, our model suggests that to be able to distinguish two materials with thermal effusivities of around 35k $(J \cdot s^{-\frac{1}{2}} \cdot K^{-1} \cdot m^{-2})$ and 20k $(J \cdot s^{-\frac{1}{2}} \cdot K^{-1} \cdot m^{-2})$ (possibly two metals, due to high effusivities), the robot with the tactile sensor needs to be in contact with the material samples for at least 3 seconds. This is for a robot with a thermal sensor with 0.05°C noise and initial temperature which is 5°C higher than the material's initial temperature (see Figs. 10 and 11).

However, note that our performance model is based on a semi-infinite solid model assumption, which assumes heat transfer from the active thermal sensor to the material sample is in one direction only. In reality, however, none of the material samples are perfectly semi-infinite though its a widely used model in these scenarios. Note that this semi-infinite solid model assumption is generally valid for a short duration which is characterized by the Fourier number of the material (Ho and Jones 2007; Yang et al. 2008a). Also, the thermal properties of a material change with temperature which we did not account for in our physics-based model. While our performance model in this work is only suitable for estimating the performance of binary classification, we can transform a multiclass classification problem to binary classification problems using the one-vs-one strategy or the one-vs-rest strategy (Bishop 2006) and predict the performance of classifiers similar to the scikit-learn implementation of multiclass SVM (Pedregosa et al. 2011).

Note in Fig. 13, the metals are more densely connected in the results with the performance model, while polymers/elastomers are more densely connected for SVM. The means that the performance model finds it difficult to distinguish among materials with larger effusivity values, such as metals/alloys, while the SVM finds it difficult to distinguish among materials with smaller effusivity values, such as polymers/elastomers. This is a function of the material effusivity resolution we chose for discretization in the simulations. For example, when we divided the range of material effusivity values into 500 equal intervals (see Section 7), each interval is of 80 effusivity. But, for polymers/elastomers which are in the low effusivity range (less than 1000), there are many materials whose effusivity ranges are smaller than the effusivity resolution (80), which can make the estimated number of indistinguishable pairs for those materials (using the performance model) less than they actually are. Discretizing the material effusivity ranges to smaller values can potentially address this but in turn, increase the computational burden.

12 CONCLUSION

We investigated the binary classification of material pairs across a wide range of materials using heat transfer based sensing. We derived a physics-based model with a statistical method to calculate the binary material recognition performance when a heated sensor touches two materials with flat surfaces. We conducted a three-part evaluation of the performance model. First, we evaluated the accuracy of performance model prediction with different thermal effusivity values by calculating and comparing $\delta(e)$ vs. e curves. Based on the evaluation result, we investigated the effect of initial conditions, contact duration, and noise on the classification algorithms expected performance. Second, we performed evaluations using simulated data from 69 materials provided in CES EduPack Level 1 database. In the third part of our evaluation, we collected real-world data using a 1-DoF robot and compared the classification performance of SVM with the model prediction. Our results provide evidence for the feasibility of using the performance model to evaluate the binary material classification performance given sensor and material thermal properties. The accuracy of our performance model during real-world tasks, for which the contact between the sensor and the material is more varied and not normal, and there is a greater variety of object and material compositions, merits further investigation.

Appendix A: Finding Sensor and Material Parameters

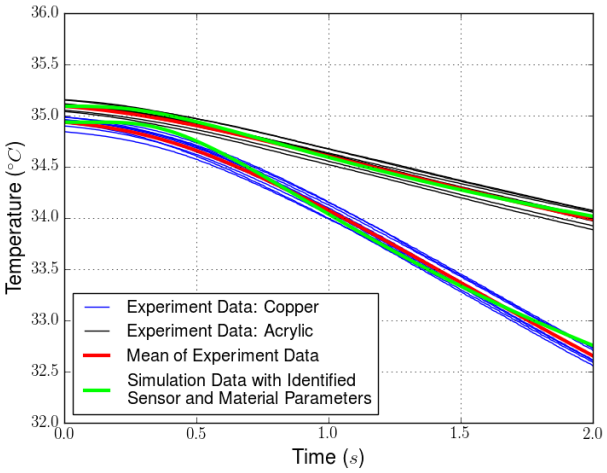

Figure 16. *Example Real-world data from Copper and Acrylic under fixed sensor initial conditions. The graphs also show the simulated data using the identified sensor and material parameters.*

To identify sensor parameter values (sensor effusivity e_{sens} and sensor diffusivity α_{sens}), we collected 10 trials of data with fixed initial conditions from each of the materials in Figure 15. Note, these 10 trials are only for identifying the sensor and material thermal properties and are not used for our material recognition experiments. We identified the sensor parameter values based on the sum of squared error between experiment temperature data and the ideal temperature data based on the semi-infinite solid model defined in Section 4.1. For each material, we used the Limited-memory BFGS with boundary constraints (L-BFGS-B) (Jones et al. 2001) algorithm to find its optimal effusivity value, with the boundary constraints given by the thermal effusivity values of materials in the CES EduPack database (Ashby 2008). In addition, since the detection of contact is based on the noisy force readings from the fabric-based force sensor, it is possible that the heat transfer started slightly before or after the estimated onset of contact. Thus, we also included a time offset from the onset of contact as an optimization parameter. We used the L-BFGS-B algorithm to find the time offset of the experiment data, and it turned out that the heat transfer started about 0.5s before the estimated onset of contact. We identified the sensor effusivity as $e_{sens} = 892\ (J \cdot s^{-\frac{1}{2}} \cdot K^{-1} \cdot m^{-2})$, and sensor diffusivity as $\alpha_{sens} = 1.19 \times 10^{-9} (m^2 \cdot s^{-1})$. Table 5 shows the identified effusivity values of all materials in this experiment.

Figure 16 shows some examples of the experimental data as well as the simulated data using the identified sensor and material thermal parameters. As seen from the figure, using

the identified parameters, the simulated data matches the experimental data well.

Appendix B: Index to Multimedia Extensions

Table of Multimedia Extensions

Extension	Type	Description
1	Video	Experiment showing the visual and infrared footage of contact between an active thermal sensor and a material sample as described in Section 9.2.

References

(2016) EPCOS (TDK) B57541G1103F NTC Thermistor 10k Bead, Glass. http://www.digikey.com/product-detail/en/epcos-tdk/B57541G1103F/495-4599-ND/3712554. Accessed: 2016-10-01.

(2016) Flexible Polyimide Foil Heater with 10 kOhm Thermistor. https://www.thorlabs.com/thorproduct.cfm?partnumber=HT10K.

Ashby MF (2008) The ces edupack database of natural and man-made materials.

Bayindir M, Abouraddy AF, Arnold J, Joannopoulos JD and Fink Y (2006) Thermal-sensing fiber devices by multimaterial codrawing. *Advanced Materials* 18(7): 845–849.

Benali-Khoudjal M, Hafez M, Alexandre JM, Benachour J and Kheddar A (2003) Thermal feedback model for virtual reality. In: *MHS2003. Proceedings of 2003 International Symposium on Micromechatronics and Human Science (IEEE Cat. No.03TH8717)*. pp. 153–158. DOI:10.1109/MHS.2003.1249925.

Bhattacharjee T, Jain A, Vaish S, Killpack MD and Kemp CC (2013) Tactile sensing over articulated joints with stretchable sensors. In: *World Haptics Conference (WHC), 2013*. IEEE, pp. 103–108.

Bhattacharjee T, Rehg JM and Kemp CC (2014) Inferring object properties from incidental contact with a tactile sensing forearm. *arXiv preprint arXiv:1409.4972* .

Bhattacharjee T, Wade J, Chitalia Y and Kemp CC (2016) Data-driven thermal recognition of contact with people and objects. In: *2016 IEEE Haptics Symposium (HAPTICS)*. IEEE, pp. 297–304.

Bhattacharjee T, Wade J and Kemp CC (2015) Material recognition from heat transfer given varying initial conditions and short-duration contact. In: *Robotics: Science and Systems (RSS)*.

Bishop CM (2006) *Pattern recognition and machine learning*, volume 1. springer New York.

Boukhanouf R, Haddad A, North M and Buffone C (2006) Experimental investigation of a flat plate heat pipe performance using {IR} thermal imaging camera. *Applied Thermal Engineering* 26(1718): 2148 – 2156. DOI: http://dx.doi.org/10.1016/j.applthermaleng.2006.04.002. URL http://www.sciencedirect.com/science/article/pii/S1359431106001293.

Caldwell DG and Gosney C (1993) Enhanced tactile feedback (tele-taction) using a multi-functional sensory system. In: *Robotics and Automation, 1993. Proceedings., 1993 IEEE International Conference on*. IEEE, pp. 955–960.

Caldwell DG and Gray JO (1993) Dynamic multi-functional tactile sensing. In: *RoManSy 9*. Springer, pp. 187–198.

Caselli S, Magnanini C and Zanichelli F (1994) Haptic object recognition with a dexterous hand based on volumetric shape representations. In: *Proceedings of the 1994 International Conference on Multisensor Fusion and Integration for Intelligent Systems*. pp. 280–287.

Castelli F (1995) An integrated tactile-thermal robot sensor with capacitive tactile array. In: *Industry Applications Conference, 1995. Thirtieth IAS Annual Meeting, IAS'95., Conference Record of the 1995 IEEE*, volume 3. IEEE, pp. 1970–1975.

Chen X, Shao F, Barnes C, Childs T and Henson B (2009) Exploring relationships between touch perception and surface physical properties. *International Journal of Design* 3(2): 67–76.

Chu V, McMahon I, Riano L, McDonald CG, He Q, Perez-Tejada JM, Arrigo M, Darrell T and Kuchenbecker KJ (2015) Robotic learning of haptic adjectives through physical interaction. *Robotics and Autonomous Systems* 63: 279–292.

Crowley ML and Krause EF (1988) Taxicab geometry, an adventure in non-euclidean geometry (p, l, s).

Dario P and De Rossi D (1985) Composite, multifunctional tactile sensor. URL https://www.google.com/patents/US4555953. US Patent 4,555,953.

Dario P, De Rossi D, Domenici C and Francesconi R (1984) Ferroelectric polymer tactile sensors with anthropomorphic features. In: *Robotics and Automation. Proceedings. 1984 IEEE International Conference on*, volume 1. IEEE, pp. 332–340.

De Maesschalck R, Jouan-Rimbaud D and Massart DL (2000) The mahalanobis distance. *Chemometrics and intelligent laboratory systems* 50(1): 1–18.

Engel J, Chen J, Fan Z and Liu C (2005) Polymer micromachined multimodal tactile sensors. *Sensors and Actuators A: Physical* 117(1): 50–61.

Engel J, Chen N, Tucker C, Liu C, Kim S and Jones D (2006) Flexible multimodal tactile sensing system for object identification. In: *Sensors, 2006. 5th IEEE Conference on*. IEEE, pp. 563–566.

Frigola-Alcade R (2015) *Bayesian Time Series Learning with Gaussian Processes*. PhD Thesis, PhD thesis, University of Cambridge.

Fudym O, Battaglia JL and Batsale JC (2005) Measurement of thermophysical properties in semi-infinite media by random heating and fractional model identification. *Review of scientific instruments* 76(4): 044902.

Gow RD, Renshaw D, Findlater K, Grant L, McLeod SJ, Hart J and Nicol RL (2007) A comprehensive tool for modeling cmos image-sensor-noise performance. *IEEE Transactions on Electron Devices* 54(6): 1321–1329.

Granta Design Ltd, Cambridge, UK (2016) Ces edupack (2016).

Hedengren K, Kornrumpf W, Miller M, Opsahl-Ong B and Uzgiris E (2001) Thermal sensor array and methods of fabrication and use. URL https://www.google.com/patents/US6180867. US Patent 6,180,867.

Herwaarden AV and Sarro P (1986) Thermal sensors based on the seebeck effect. *Sensors and Actuators* 10(3):

Table 5. Thermal Effusivity Values of Materials in the Experiment

Material	Thermal effusivity identified $(J \cdot s^{-\frac{1}{2}} \cdot K^{-1} \cdot m^{-2})$	Maximum thermal effusivity from database $(J \cdot s^{-\frac{1}{2}} \cdot K^{-1} \cdot m^{-2})$	Minimum thermal effusivity from database $(J \cdot s^{-\frac{1}{2}} \cdot K^{-1} \cdot m^{-2})$
Cardboard	336.90	196.67	452.23
Wood	400.95	331.00	506.46
ABS	514.15	514.15	882.58
Rubber	570.81	407.00	570.81
MDF	544.63	618.47	733.93
Acrylic	635.49	380.35	702.15
Porcelain	1276.59	1162.69	1334.07
Glass	1433.31	1433.31	1560.39
Granite	2749.87	2252.32	2749.87
Stainless Steel	10184.17	6388.35	10184.17
Aluminum	17530.03	12767.69	25972.02
Copper	23049.18	23049.18	36761.16

321 – 346. DOI:http://dx.doi.org/10.1016/0250-6874(86)80053-1. URL http://www.sciencedirect.com/science/article/pii/0250687486800531.

Ho H and Jones LA (2004) Material identification using real and simulated thermal cues. In: *The 26th Annual International Conference of the IEEE Engineering in Medicine and Biology Society*, volume 1. pp. 2462–2465. DOI:10.1109/IEMBS.2004.1403711.

Ho HN and Jones LA (2006) Thermal model for hand-object interactions. In: *2006 14th Symposium on Haptic Interfaces for Virtual Environment and Teleoperator Systems*. pp. 461–467. DOI:10.1109/HAPTIC.2006.1627108.

Ho HN and Jones LA (2007) Development and evaluation of a thermal display for material identification and discrimination. *ACM Transactions on Applied Perception (TAP)* 4(2): 13.

Ho HN and Jones LA (2008) Modeling the thermal responses of the skin surface during hand-object interactions. *Journal of Biomechanical Engineering* 130(2): 021005.

Hogervorst MA, Bijl P and Valeton JM (2001) Capturing the sampling effects: a tod sensor performance model. In: *Proc. SPIE*, volume 4372. pp. 62–73.

Jackson W, Biegelsen D, Berlin A, Sprague R and Cass T (1999) Paper property sensing system. URL https://www.google.com/patents/US5934140. US Patent 5,934,140.

Jannot Y and Meukam P (2004) Simplified estimation method for the determination of the thermal effusivity and thermal conductivity using a low cost hot strip. *Measurement Science and Technology* 15(9): 1932. URL http://stacks.iop.org/0957-0233/15/i=9/a=034.

Johnson N (1972) S. kotz distributions in statistics: continuous multivariate distributions.

Jones E, Oliphant T and Peterson P (2001) Scipy: Open source scientific tools for python. *http://www. scipy. org/* .

Jones LA and Ho HN (2008) Warm or cool, large or small? the challenge of thermal displays. *IEEE Transactions on Haptics* 1(1): 53–70. DOI:10.1109/TOH.2008.2.

Kabov O and Marchuk I (1996) Thermal imaging study of the liquid film flowing on vertical surface with local heat source. *Russian Journal of Engineering Thermophysics* 6(2): 105–138.

Kaplan H (2007) *Practical Applications of Infrared Thermal Sensing and Imaging Equipment*. 3 edition. The address: SPIE Press. ISBN 9780819467232.

Kerr E, McGinnity TM and Coleman S (2013) Material classification based on thermal properties-a robot and human evaluation. In: *Robotics and Biomimetics (ROBIO), 2013 IEEE International Conference on*. IEEE, pp. 1048–1053.

Kim J, Lee M, Shim HJ, Ghaffari R, Cho HR, Son D, Jung YH, Soh M, Choi C, Jung S, Chu K, Jeon D, Lee ST, Kim JH, Choi SH, Hyeon T and Kim DH (2014) Stretchable silicon nanoribbon electronics for skin prosthesis. *Nature Communications* 5: 5747 EP –. URL http://dx.doi.org/10.1038/ncomms6747. Article.

Krapels K, Driggers RG, Deaver D, Moyer SK and Palmer J (2007) Midwave infrared and visible sensor performance modeling: small craft identification discrimination criteria for maritime security. *applied optics* 46(30): 7345–7353.

Lienhard JH (2011) *A heat transfer textbook*. Dover Civil and Mechanical Engineering, 4th ed.. edition. Mineola, N.Y.: Dover Publications. ISBN 9780486318370.

Lin CH, Erickson TW, Fishel JA, Wettels N and Loeb GE (2009) Signal processing and fabrication of a biomimetic tactile sensor array with thermal, force and microvibration modalities. In: *Robotics and Biomimetics (ROBIO), 2009 IEEE International Conference on*. IEEE, pp. 129–134.

Liu C, Chen J and Engel J (2008) Sensor chip and apparatus for tactile and/or flow sensing. URL https://www.google.com/patents/US7357035. US Patent 7,357,035.

Ma B, Ren J, Deng J and Yuan W (2010) Flexible thermal sensor array on pi film substrate for underwater applications. In: *2010 IEEE 23rd International Conference on Micro Electro Mechanical Systems (MEMS)*. pp. 679–682. DOI:10.1109/MEMSYS.2010.5442315.

Mansky P and Bennett J (2002) Method for conducting sensor array-based rapid materials characterization. URL https://www.google.com/patents/US6438497. US Patent 6,438,497.

Mansky P and Bennett J (2003) Sensor array-based system and method for rapid materials characterization. URL http://google.com/patents/US6535824. US Patent 6,535,824.

Mathis NE (2000) New transient non-destructive technique measures thermal effusivity and diffusivity. *Thermal Conductivity* 25: 3–14.

Matian M, Marquis A and Brandon N (2010) Application of thermal imaging to validate a heat transfer model for polymer electrolyte fuel cells. *International Journal of Hydrogen Energy* 35(22): 12308 – 12316. DOI: http://dx.doi.org/10.1016/j.ijhydene.2010.08.041. URL http://www.sciencedirect.com/science/article/pii/S0360319910016800. Bio-Ethanol and Other Renewable Sources and Reforming Process for Sustainable Hydrogen Production.

McMahon I, Chu V, Riano L, McDonald G, He Q, Perez-Tejada J, Arrigo M, Fitter N, Nappo J, Darrell T and Kuchenbecker K (2012) Robotic learning of haptic adjectives through physical interaction. In: *Proceedings of the 2012 Second Workshop on Advances in Tactile Sensing and Touch-based Human-Robot Interaction*.

Mittendorfer P and Cheng G (2011) Humanoid multimodal tactile-sensing modules. *Robotics, IEEE Transactions on* 27(3): 401–410.

Monkman GJ and Taylor PM (1993) Thermal tactile sensing. *Robotics and Automation, IEEE Transactions on* 9(3): 313–318.

Mulaveesala R, Ghali VS and Arora V (2013) Applications of non-stationary thermal wave imaging methods for characterisation of fibre-reinforced plastic materials. *Electronics Letters* 49(2): 118–119. DOI:10.1049/el.2012.3844.

Nadarajah S (2005) A generalized normal distribution. *Journal of Applied Statistics* 32(7): 685–694.

Patnaik P (1949) The non-central χ2-and f-distributions and their applications. *Biometrika* 36(1-2): 202–232.

Pav SE (2017) *sadists: Some Additional Distributions*. URL https://github.com/shabbychef/sadists. R package version 0.2.3.

Pedregosa F, Varoquaux G, Gramfort A, Michel V, Thirion B, Grisel O, Blondel M, Prettenhofer P, Weiss R, Dubourg V, Vanderplas J, Passos A, Cournapeau D, Brucher M, Perrot M and Duchesnay E (2011) Scikit-learn: Machine learning in Python. *Journal of Machine Learning Research* 12: 2825–2830.

Petrovi V and Xydeas C (2000) On the effects of sensor noise in pixel-level image fusion performance. In: *Information Fusion, 2000. FUSION 2000. Proceedings of the Third International Conference on*, volume 2. IEEE, pp. WEC3–14.

Planck M (2013) *The theory of heat radiation*. Courier Corporation.

Rasmussen CE (2004) Gaussian processes in machine learning. In: *Advanced lectures on machine learning*. Springer, pp. 63–71.

Russell RA (1985) A thermal sensor array to provide tactile feedback for robots. *The International journal of robotics research* 4(3): 35–39.

Sarro P, Yashiro H, Herwaarden A and Middelhoek S (1988) An integrated thermal infrared sensing array. *Sensors and Actuators* 14(2): 191 – 201. DOI: http://dx.doi.org/10.1016/0250-6874(88)80065-9. URL http://www.sciencedirect.com/science/article/pii/0250687488800659.

Schaufelbuhl A, Schneeberger N, Munch U, Waelti M, Paul O, Brand O, Baltes H, Menolfi C, Huang Q, Doering E and Loepfe M (2001) Uncooled low-cost thermal imager based on micromachined cmos integrated sensor array. *Journal of Microelectromechanical Systems* 10(4): 503–510. DOI: 10.1109/84.967372.

Shao F, Chen X, Barnes C and Henson B (2010) A novel tactile sensation measurement system for qualifying touch perception. *Proceedings of the Institution of Mechanical Engineers, Part H: Journal of Engineering in Medicine* 224(1): 97–105.

Shih WP, Tsao LC, Lee CW, Cheng MY, Chang C, Yang YJ and Fan KC (2010) Flexible temperature sensor array based on a graphite-polydimethylsiloxane composite. *Sensors* 10(4): 3597–3610. DOI:10.3390/s100403597. URL http://www.mdpi.com/1424-8220/10/4/3597.

Siegel D, Garabieta I and Hollerbach JM (1986) An integrated tactile and thermal sensor. In: *Robotics and Automation. Proceedings. 1986 IEEE International Conference on*, volume 3. IEEE, pp. 1286–1291.

Someya T, Kato Y, Sekitani T, Iba S, Noguchi Y, Murase Y, Kawaguchi H and Sakurai" T (2005) Conformable, flexible, large-area networks of pressure and thermal sensors with organic transistor active matrixes. *Proc. Natl. Acad. Sci. U.S.A* 102(2): 12321 – 12325. DOI:10.1073/pnas.0502392102. URL http://www.pnas.org/content/102/35/12321.abstract?tab=author-info.

Syntouch (2015) *Syntouch BioTac Sensor*. Syntouch Inc. URL https://www.syntouchinc.com/wp-content/uploads/2017/01/BioTac_Product_Manual.pdf.

Taddeucci D, Laschi C, Lazzarini R, Magni R, Dario P and Starita A (1997) An approach to integrated tactile perception. In: *Proceedings of International Conference on Robotics and Automation*, volume 4. pp. 3100–3105 vol.4. DOI:10.1109/ROBOT.1997.606759.

Takamuku S, Iwase T and Hosoda K (2008) Robust material discrimination by a soft anthropomorphic finger with tactile and thermal sense. In: *Intelligent Robots and Systems, 2008. IROS 2008. IEEE/RSJ International Conference on*. IEEE, pp. 3977–3982.

Tong A (2001) Improving the accuracy of temperature measurements. *Sensor Review* 21(3): 193–198. DOI:10.1108/02602280110398044. URL http://dx.doi.org/10.1108/02602280110398044.

VanDamme GE and McGarvey JW (1972) Infrared nondestructive testing of laminated structures and electrical circuits. Technical report. URL http://oai.dtic.mil/oai/oai?verb=getRecord&metadataPrefix=html&identifier=AD0746233.

Wade J, Bhattacharjee T and Kemp CC (2016) Force and thermal sensing with a fabric-based skin. In: *See, Touch and Hear: 2nd Workshop on multimodal sensor-based robot control for HRI and soft manipulation, IEEE/RSJ International Conference on Intelligent Robots and Systems (IROS)*.

Wettels N, Santos VJ, Johansson RS and Loeb GE (2008) Biomimetic tactile sensor array. *Advanced Robotics* 22(8): 829–849.

Xu D, Loeb GE and Fishel JA (2013) Tactile identification of objects using bayesian exploration. In: *Robotics and Automation (ICRA), 2013 IEEE International Conference on*. IEEE, pp. 3056–3061.

Yamamoto A, Cros B, Hashimoto H and Higuchi T (2004) Control of thermal tactile display based on prediction of contact temperature. In: *Robotics and Automation, 2004. Proceedings.*

ICRA '04. 2004 IEEE International Conference on, volume 2. pp. 1536–1541 Vol.2. DOI:10.1109/ROBOT.2004.1308042.

Yang GH, Jones LA and Kwon DS (2008a) Use of simulated thermal cues for material discrimination and identification with a multi-fingered display. *Presence: Teleoperators and Virtual Environments* 17(1): 29–42.

Yang YJ, Cheng MY, Chang WY, Tsao LC, Yang SA, Shih WP, Chang FY, Chang SH and Fan KC (2008b) An integrated flexible temperature and tactile sensing array using pi-copper films. *Sensors and Actuators A: Physical* 143(1): 143 – 153. DOI:http://dx.doi.org/10.1016/j.sna.2007.10.077. URL `http://www.sciencedirect.com/science/article/pii/S0924424707008126`. Micromechanics Section of Sensors and Actuators (SAMM), based on contributions revised from the Technical Digest of the {IEEE} 20th International Conference on Micro Electro Mechanical Systems (MEMS 2007)MEMS 2007IEEE 20th International Conference on Micro Electro Mechanical Systems.

Yang YJ, Cheng MY, Shih SC, Huang XH, Tsao CM, Chang FY and Fan KC (2010) A 32$\times$ 32 temperature and tactile sensing array using pi-copper films. *The International Journal of Advanced Manufacturing Technology* 46(9-12): 945–956.

Yuji JI and Shida K (2000) A new multifunctional tactile sensing technique by selective data processing. *Instrumentation and Measurement, IEEE Transactions on* 49(5): 1091–1094.

Yunus C and Afshin G (2010) Transient heat conduction. In: *Heat and Mass Transfer: Fundamentals and Applications*, chapter 4. New York, NY: McGraw-Hill, pp. 245–246.

Funding

This work was supported in part by NSF Awards EFRI-1137229 and IIS-1150157, the National Institute on Disability, Independent Living, and Rehabilitation Research (NIDILRR) grant 90RE5016-01-00 via RERC TechSAge, and a Google Faculty Research Award.